Eur. Phys. J. C (2012) 72:2218
DOI 10.1140/epjc/s10052-012-2218-4

THE EUROPEAN PHYSICAL JOURNAL C

Regular Article - Theoretical Physics

Galaxy cluster number count data constraints on cosmological parameters

L. Campanelli[1,a], **G.L. Fogli**[1,2,b], **T. Kahniashvili**[3,4,5,c], **A. Marrone**[1,2,d], **Bharat Ratra**[6,e]

[1]Dipartimento di Fisica, Università di Bari, 70126 Bari, Italy
[2]INFN-Sezione di Bari, 70126 Bari, Italy
[3]McWilliams Center for Cosmology and Department of Physics, Carnegie Mellon University, 5000 Forbes Ave, Pittsburgh, PA 15213, USA
[4]Department of Physics, Laurentian University, Ramsey Lake Road, Sudbury, ON P3E 2C, Canada
[5]Abastumani Astrophysical Observatory, Ilia State University, 2A Kazbegi Ave, Tbilisi, 0160, Georgia
[6]Department of Physics, Kansas State University, 116 Cardwell Hall, Manhattan, KS 66506, USA

Received: 28 August 2012 / Revised: 16 October 2012 / Published online: 10 November 2012
© Springer-Verlag Berlin Heidelberg and Società Italiana di Fisica 2012

Abstract We use data on massive galaxy clusters ($M_{\rm cluster} > 8 \times 10^{14} h^{-1} M_\odot$ within a comoving radius of $R_{\rm cluster} = 1.5 h^{-1}$ Mpc) in the redshift range $0.05 \lesssim z \lesssim 0.83$ to place constraints, simultaneously, on the nonrelativistic matter density parameter Ω_m, on the amplitude of mass fluctuations σ_8, on the index n of the power-law spectrum of the density perturbations, and on the Hubble constant H_0, as well as on the equation-of-state parameters (w_0, w_a) of a smooth dark energy component.

For the first time, we properly take into account the dependence on redshift and cosmology of the quantities related to cluster physics: the critical density contrast, the growth factor, the mass conversion factor, the virial overdensity, the virial radius and, most importantly, the cluster number count derived from the observational temperature data.

We show that, contrary to previous analyses, cluster data alone prefer low values of the amplitude of mass fluctuations, $\sigma_8 \leq 0.69$ (1σ C.L.), and large amounts of nonrelativistic matter, $\Omega_m \geq 0.38$ (1σ C.L.), in slight tension with the ΛCDM concordance cosmological model, though the results are compatible with ΛCDM at 2σ. In addition, we derive a σ_8 normalization relation, $\sigma_8 \Omega_m^{1/3} = 0.49 \pm 0.06$ (2σ C.L.).

Combining cluster data with σ_8-independent baryon acoustic oscillation observations, cosmic microwave background data, Hubble constant measurements, Hubble parameter determination from passively evolving red galaxies, and magnitude–redshift data of type Ia supernovae, we find $\Omega_m = 0.28^{+0.03}_{-0.02}$ and $\sigma_8 = 0.73^{+0.03}_{-0.03}$, the former in agreement and the latter being slightly lower than the corresponding values in the concordance cosmological model. We also find $H_0 = 69.1^{+1.3}_{-1.5}$ km/s/Mpc, the fit to the data being almost independent on n in the adopted range [0.90, 1.05].

Concerning the dark energy equation-of-state parameters, we show that the present data on massive clusters weakly constrain (w_0, w_a) around the values corresponding to a cosmological constant, i.e. $(w_0, w_a) = (-1, 0)$. The global analysis gives $w_0 = -1.14^{+0.14}_{-0.16}$ and $w_a = 0.85^{+0.42}_{-0.60}$ (1σ C.L. errors). Very similar results are found in the case of time-evolving dark energy with a constant equation-of-state parameter $w = \text{const}$ (the XCDM parametrization). Finally, we show that the impact of bounds on (w_0, w_a) is to favor top-down phantom models of evolving dark energy.

1 Introduction

In the last few years galaxy cluster observations have begun to provide useful constraints on cosmological parameters (for a recent review see Ref. [1]). Data on galaxy clusters are now used to test the validity of the standard cosmological model, the so-called Λ cold dark matter (ΛCDM) concordance model, [2], which describes observational data at large cosmological scales (from galactic scales to the present horizon scale) reasonably well [3]. In particular, cluster observations can help tighten the bounds on cosmological parameters such as the nonrelativistic matter density parameter Ω_m, the amplitude of mass fluctuations σ_8, the power-law index n of the density perturbation power spectrum, and the Hubble constant H_0 [4].

When combined with other cosmological probes—such as cosmic microwave background (CMB) radiation aniso-

[a] e-mail: leonardo.campanelli@ba.infn.it
[b] e-mail: gianluigi.fogli@ba.infn.it
[c] e-mail: tinatin@phys.ksu.edu
[d] e-mail: antonio.marrone@ba.infn.it
[e] e-mail: ratra@phys.ksu.edu

tropy, baryon acoustic oscillations (BAO) in the matter power spectrum, Hubble parameter, and type Ia supernovae (SNeIa) data—galaxy cluster observations provide a unique insight towards helping understand the evolution of the Universe, from the inflation era to today.

Despite the observational success of the ΛCDM model, a number of basic questions remain unanswered. Dark energy is a major mystery (for reviews on dark energy and modified gravity see, e.g., Refs. [5–10]). A possibility is that dark energy is simply a manifestation of a nonzero vacuum energy, a cosmological constant Λ,[1] but dynamical scalar-field models of dark energy, [16, 17], are also compatible with present data.[2]

Measurements of the local abundance and growth of galaxy clusters from X-ray [18–22] and optical [23] surveys have been recently used to probe the standard cosmological model. In particular, the emerging picture is that a cosmological constant still remains a good candidate for dark energy. This conclusion does not exclude the possibility that future cluster surveys will allow us to discriminate between the ΛCDM model and dynamical dark energy models [24–27].

The aim of this paper is to use present data on massive galaxy clusters ($M_{\rm cluster} > 8 \times 10^{14} h^{-1} M_{\odot}$ within a comoving radius of $R_{\rm cluster} = 1.5 h^{-1}$ Mpc) at low and high redshifts ($0.05 \lesssim z \lesssim 0.83$) to constrain some of the free parameters of the standard cosmological model, and to investigate the possibility that the dark energy density evolves in time, instead of staying constant.

It is worth noticing that the evolution with redshift of massive clusters is very sensitive to the cosmological parameters, especially to σ_8 and Ω_m [28, 29]. In particular, the abundance of massive clusters depends exponentially on σ_8, in such a way that high values of σ_8 favor the formation of structures at early times, while a low amplitude of mass fluctuations results in few massive clusters forming at high redshifts.

In Refs. [28, 29] these data were used to determine the linear amplitude of mass fluctuations and the nonrelativistic matter density in a Universe with a cosmological constant. We extend the analysis of Refs. [28, 29] to the case of evolving dark energy, and we properly take into account the dependence on redshift and cosmology of quantities related to cluster physics, such as the critical density contrast, the growth factor, the mass conversion factor, the virial overdensity, and the virial radius. Most importantly, we consider the dependence on redshift and cosmology of the cluster number count derived from the observational data. We emphasize that the observed number of clusters with masses exceeding a fixed threshold is calculated as the number of clusters with X-ray temperature larger than a corresponding temperature threshold, and that the relation between mass and temperature depends on the redshift and cosmological parameters.

It is of great interest to determine if the dark energy is well-approximated by a cosmological constant or if it decreases slowly in time (and so varies weakly in space). Ideally one would very much prefer a model-independent resolution of this issue. However, at this point in time, observational data are not up to this task. One must instead use the available observational data to constrain model parameters and so determine if the cosmological constant point in model parameter space is or is not favored over points where the dark energy density slowly decreases in time. While it is useful to perform such an analysis using a consistent and physically motivated model, such as the inverse power-law potential energy density scalar-field model [16, 17], this is computationally quite demanding, so here we make use of a simple parametrization of time-evolving dark energy in a preliminary attempt to investigate this matter.

In order to discriminate between a cosmological constant and dynamical dark energy we use the dark energy equation-of-state parameter parametrization [30, 31]

$$w(a) = w_0 + w_a(1 - a), \tag{1}$$

where a is the scale factor related to the redshift z by $a = 1/(1 + z)$. The cosmological constant corresponds to $w_0 = -1$ and $w_a = 0$, the case of constant equation of state corresponds to $w_0 = w = \text{const}$ and $w_a = 0$ (known as the XCDM parametrization of time-evolving dark energy), while the general case of time-evolving dark energy corresponds to $w_a \neq 0$.

In this paper, we consider the case of a smooth dark energy component, namely the case where the dark energy does not cluster. For clustering dark energy, it could be expected that the bounds on dark energy equation-of-state parameters w_0, w_a, as well as on the cosmological parameters

[1] It has been known for some time that a spatially flat ΛCDM model is consistent with most observational constraints, see, e.g., Refs. [11–13]. In the ΛCDM model the energy budget is dominated by far by a cosmological constant, a spatially homogeneous fluid with equation-of-state parameter $w_\Lambda = p_\Lambda/\rho_\Lambda = -1$ (where p_Λ and ρ_Λ are the fluid pressure and energy density), with nonrelativistic CDM being the second largest contributor. Note that the "standard" CDM structure formation model—which the standard ΛCDM cosmological model assumes—might have some observational inconsistencies (see, e.g., [14, 15]).

[2] In dynamical dark energy models the dark energy density decreases in time and so remains comparable to the nonrelativistic matter (CDM and baryons) energy density for a longer time (than does a time-independent Λ). This partially alleviates the "coincidence" puzzle of the ΛCDM model. In addition, some dynamical dark energy scalar-field models have a nonlinear attractor solution that generates the current, tiny, dark energy density energy scale of order an meV from a significantly higher energy density scale (possibly of a more fundamental model) as a consequence of the very slow decrease in time of the dark energy density during the very long age of the Universe. These results are often viewed as providing significant theoretical motivation to consider dynamical dark energy models [16, 17].

(Ω_m, σ_8), will be weakened because of the degeneracy between the above parameters and the effective dark energy sound speed (which parameterizes the level of dark energy clustering) [32].

The plan of our paper is as follows. In the next section, we introduce the basic theory and data on galaxy cluster number counts used in our analysis. In Sect. 3, we present data from other types of cosmological probe: baryon acoustic oscillations, cosmic microwave background radiation anisotropies, passively evolving red galaxies, and type Ia supernovae. In Sect. 4, we outline a joint analysis of all data and discuss the results on the (Ω_m, σ_8) and (w_0, w_a) planes, and in the XCDM case. In Sect. 5, we briefly discuss the impact of our results on some models of evolving dark energy. In Sect. 6, we draw our conclusions. Finally, in the Appendices we discuss in detail the critical density contrast and the growth factor (Appendix A), the mass conversion factor (Appendix B), and the virial overdensity and the virial radius (Appendix C).

2 Galaxy cluster number counts

In this section we introduce the basic physical quantities and observables related to galaxy cluster number counts and we discuss the available experimental data.

2.1 Theory

Cluster number and comoving volume The comoving number of clusters in the redshift interval $[z_1, z_2]$, whose mass M is greater than a fiducial mass M_0, is

$$\mathcal{N} = \int_{z_1}^{z_2} dz \frac{dV(z)}{dz} N(M > M_0, z), \tag{2}$$

where

$$V(z) = 4\pi \int_0^z dz' \frac{d_L^2(z')}{(1+z')^2 H(z')} \tag{3}$$

is the comoving volume at redshift z, and

$$d_L(z) = (1+z) \int_0^z \frac{dz'}{H(z')} \tag{4}$$

is the luminosity distance with $H(z)$ the Hubble parameter. The "mass function" $N(M > M_0, z)$ appearing in Eq. (2) represents the comoving cluster number density at redshift z of clusters with masses greater than M_0.

For a cosmological model with evolving dark energy equation-of-state parameter of the form (1), the Hubble parameter normalized to its present value H_0 is

$$E(z) = \frac{H(z)}{H_0} = \left[\frac{\rho_m(z)}{\rho_{\rm cr}^{(0)}} + \frac{\rho_{\rm DE}(z)}{\rho_{\rm cr}^{(0)}} \right]^{1/2}. \tag{5}$$

The quantities

$$\rho_m(z) = \Omega_m \rho_{\rm cr}^{(0)} (1+z)^3 \tag{6}$$

and

$$\rho_{\rm DE}(z) = \Omega_{\rm DE} \rho_{\rm cr}^{(0)} (1+z)^{3(1+w_0+w_a)} e^{-3w_a z/(1+z)} \tag{7}$$

are the energy densities of nonrelativistic matter and dark energy, respectively. Here, $\Omega_m = \rho_m^{(0)}/\rho_{\rm cr}^{(0)}$ and $\Omega_{\rm DE} = \rho_{\rm DE}^{(0)}/\rho_{\rm cr}^{(0)}$ are the matter and dark energy density parameters, and $\rho_m^{(0)}$, $\rho_{\rm DE}^{(0)}$, and $\rho_{\rm cr}^{(0)} = 3H_0^2/(8\pi G)$ are the present matter, dark energy, and critical energy densities, respectively, while G is the Newton constant.

In this paper, for computational simplicity, we restrict ourselves to the case of a flat universe,[3] so

$$\Omega_m + \Omega_{\rm DE} = 1. \tag{8}$$

Mass function To compute the mass function, we use the Press–Schechter (PS) approach [35], as modified by Sheth and Tormen (ST) [36]. In this approach, the mass function is written as

$$N(M > M_0, z) = \int_{M_0}^{\infty} dM\, n(M, z), \tag{9}$$

and

$$M = \frac{4\pi}{3} r^3(z) \rho_m(z) = \frac{4\pi}{3} R^3 \rho_m^{(0)} \tag{10}$$

is the mass within a sphere of physical radius $r(z)$, whose corresponding comoving radius is $R = (1+z)r(z)$.

In Eq. (9), $n(M, z)\, dM$ is the comoving number density at redshift z of clusters with masses in the interval $[M, M + dM]$, and is written as

$$n = \frac{2\rho_m}{M} \nu f(\nu) \frac{d\nu}{dM}. \tag{11}$$

Here the multiplicity function $\nu f(\nu)$ is (in the PS and ST models) an universal function of the peak height

$$\nu = \frac{\delta_c}{\sigma}, \tag{12}$$

and is normalized as

$$\int_0^{\infty} d\nu\, \nu f(\nu) = \frac{1}{2}. \tag{13}$$

The functional form of $\nu f(\nu)$ is discussed below. The critical density contrast $\delta_c(z)$ is the density contrast for a linear overdensity able to collapse at the redshift z, and its dependence on cosmological parameters is discussed in Appendix A.

The root mean square (rms) amplitude σ of density fluctuations in a sphere of comoving radius R, whose corresponding physical radius r contains the mass M, is related to the matter power spectrum of density perturbations at redshift z, $P(k, z)$, through

$$\sigma^2(R, z) = \frac{1}{2\pi^2} \int_0^{\infty} dk\, k^2 P(k, z) W^2(kR). \tag{14}$$

[3] This is consistent with the simplest interpretation of the CMB anisotropy data, see, e.g. [33, 34].

Here

$$W(x) = \frac{3(\sin x - x\cos x)}{x^3} \tag{15}$$

is the Fourier transform of the top-hat window function and

$$P(k,z) = P_0(k)T^2(k)D^2(z), \tag{16}$$

with $D(z)$ being the growth factor (discussed in Appendix A) and $T(k)$ the transfer function.

We assume that the post-inflationary density perturbation power spectrum $P_0(k)$ is a simple power law,

$$P_0(k) = Ak^n, \tag{17}$$

with the scale-invariant spectrum corresponding to $n = 1$. The normalization constant A is a free parameter of the model and can be expressed as a function of the other cosmological parameters (see below, footnote 4), while the total transfer function $T(k)$ is taken from Ref. [37]. The transfer function depends on H_0 and on baryon and cold dark matter density parameters Ω_b and Ω_c. The total amount of matter is given by $\Omega_m = \Omega_b + \Omega_c$ and in this paper we take $\Omega_b h^2 = 0.02$, with h defined by

$$H_0 = 100h \text{ km/s/Mpc}. \tag{18}$$

In the Press–Schechter parametrization, the form of the multiplicity function is a result of the assumption that initial density fluctuations are Gaussian: $\nu f(\nu) = e^{-\nu^2/2}/\sqrt{2\pi}$. In this paper, however, we use the form

$$\nu f(\nu) = K\left[1 + \left(a\nu^2\right)^{-p}\right]e^{-a\nu^2/2}, \tag{19}$$

introduced by Sheth and Tormen, inspired by a model of elliptical collapse. The constant

$$K = \frac{\sqrt{a}}{\sqrt{2\pi} + 2^{1/2-p}\Gamma(1/2-p)} \tag{20}$$

results from the normalization condition (13), $\Gamma(x)$ is the Gamma function, while a and p are phenomenological constants to be determined by fitting to N-body simulation results. We use the values found by Sheth and Tormen, namely $a = 0.707$ and $p = 0.3$. (The Press–Schechter case is recovered for $a = 1$ and $p = 0$.)

Finally, putting all this together, we can rewrite the mass function as

$$\begin{aligned} N(M > M_0, z) &= 2K\frac{\rho_m(z)}{M_0}\frac{\delta_c(z)}{\sigma_8 D(z)}\int_1^\infty \frac{dx}{x^3}\frac{1}{\Sigma^2(x)}\left|\frac{d\Sigma(x)}{dx}\right| \\ &\quad\times\left\{1 + \left[\frac{a\delta_c^2(z)}{\sigma_8^2 D^2(z)\Sigma^2(x)}\right]^{-p}\right\} \\ &\quad\times\exp\left[-\frac{a\delta_c^2(z)}{2\sigma_8^2 D^2(z)\Sigma^2(x)}\right], \end{aligned} \tag{21}$$

where we have introduced the function

$$\Sigma^2(x) = \frac{\int_0^\infty dy\, y^{n+2}T^2(y/R_8)W^2(xyR_0/R_8)}{\int_0^\infty dy\, y^{n+2}T^2(y/R_8)W^2(y)}, \tag{22}$$

and the quantities[4]

$$\begin{aligned} &\sigma_8 = \sigma(R_8, 0), \\ &R_8 = 8h^{-1}\text{ Mpc}, \\ &R_0 = \left(\frac{3M_0}{4\pi\rho_m^{(0)}}\right)^{1/3}. \end{aligned} \tag{23}$$

We note that the function $\Sigma(x)$ evaluated at $x = R/R_0$ is the present value of the rms amplitude σ at the scale R normalized to its present value at the scale R_8:

$$\Sigma(R/R_0) = \frac{\sigma(R,0)}{\sigma_8}. \tag{24}$$

This result will be used in Appendix A.

2.2 Data

Data on cluster abundance at different redshifts can be expressed as the comoving number of clusters in the redshift interval $[z_1, z_2]$, with mass M' within a reference comoving radius R_0' greater than a fiducial mass M_0' within the same radius. Here and in the following, a prime is used to distinguish quantities related to observed masses and radii from theoretical ones, discussed in the previous subsection. We follow Refs. [28, 29] and take

$$R_0' = 1.5h^{-1}\text{ Mpc}, \tag{25}$$

$$M_0' = 8\times 10^{14}h^{-1}M_\odot, \tag{26}$$

where $M_\odot \simeq 1.989\times 10^{33}$ g is the solar mass.

Only an effective fraction $\alpha(z)$ of the total comoving volume at redshift z is observed, so the expected comoving number of clusters in the redshift interval $[z_1, z_2]$, with mass M' greater than M_0', is

$$\mathcal{N}' = \int_{z_1}^{z_2} dz\,\frac{d[\alpha(z)V(z)]}{dz}N'\left(M' > M_0', z\right), \tag{27}$$

where $N'(M' > M_0', z)$ represents the comoving cluster number density at redshift z of clusters with masses M' greater than M_0'. The mass function $N'(M' > M_0', z)$ can be written as

$$N'\left(M' > M_0', z\right) = \int_{M_0'}^\infty dM'\, n'\left(M', z\right). \tag{28}$$

Here $n'(M', z)dM'$ is the comoving number density at redshift z of clusters with masses M' in the interval $[M', M' + dM']$, and is defined by

$$n'\left(M', z\right)dM' = n(M, z)\,dM, \tag{29}$$

where $n(M, z)$ is given by Eq. (11).

[4] As anticipated, the normalization constant A can be related to the other cosmological parameters, Ω_b, Ω_c, h, and n: $A = 2\pi^2\sigma_8^2 R_8^{n+3}/\int_0^\infty dy\, y^{n+2}T^2(y/R_8)W^2(y)$.

Inserting Eq. (29) in Eq. (28) we obtain

$$N'\big(M' > M'_0, z\big) = \int_{g(M'_0)}^{\infty} dM\, n(M, z), \tag{30}$$

where the function g relates the observed mass M' to the virial mass M in the PS or ST parametrization. Consequently, $g(M'_0)$ is the fiducial virial mass

$$M_0 = g\big(M'_0\big) \tag{31}$$

which corresponds to the fiducial mass M'_0 adopted in the observations. In Appendix B we describe the procedure that gives the mass M_0 as a function of M'_0. In general, the function g depends on the redshift and cosmological parameters.

In Table 1, we show the four redshift bins $[z_1^{(i)}, z_2^{(i)}]$ $(i = 1, 2, 3, 4)$, centered at $z_c^{(i)}$, of the massive clusters data. Also listed are the values of the effective fraction of the observed comoving volume of each bin, α_i. The α_i values are for a cosmology with $(\Omega_m, w) = (0.3, -1)$, and were computed using the results of Refs. [28, 29].

The α_i parameters depend, in principle, on the cosmology and their values can be obtained using the $\Sigma(1/V_{\max})$ method applied to observational data [38–41]. However, the dependence of α_i on the cosmology is weak compared to that of the comoving volume. Using the results of Refs. [28, 29] we get, for example, that passing from the cosmology with $(\Omega_m, w) = (0.3, -1)$ to that with $\Omega_m = 1$, the percentage variation of the comoving volume relative to the third bin, $V(z_2^{(3)}) - V(z_1^{(3)})$, is 117 %, while that of α_3 is about 1 %. Similar results hold for the other bins.

References [28, 29, 38, 39, 42] give X-ray temperature measurements for massive clusters. For completeness we show these data in Table 2.

In order to convert temperature to mass, we use the mass–temperature conversion formula of Refs. [43, 44] (see Ref. [45] for a different approach to the problem of cluster mass–temperature conversion):

$$M(<r) = 10^{14} M_\odot\, \kappa_\Delta \frac{T_X}{\mathrm{keV}} \frac{r}{\mathrm{Mpc}}, \tag{32}$$

where $M(<r)$ is the mass within a physical radius r, T_X is the cluster X-ray temperature, and κ_Δ is a parameter which depends only on Δ'_v. Here Δ'_v is the virial overdensity relative to the critical density. It is related to the virial overdensity relative to the background matter density, Δ_v, through

$$\Delta'_v = \frac{\Omega_m (1+z)^3}{E^2(z)} \Delta_v. \tag{33}$$

Table 1 The four redshift intervals $[z_1^{(i)}, z_2^{(i)}]$ $(i = 1, 2, 3, 4)$, centered at $z_c^{(i)}$, of the massive clusters data and the references from which data have been taken. α_i is the effective fraction of the observed comoving volume of the ith bin and the values listed here are for the case with $\Omega_m = 0.3$ and $w = -1$

bin i	$z_1^{(i)}$	$z_2^{(i)}$	$z_c^{(i)}$	Ref.	α_i
1	0.00	0.10	0.050	[38]	0.309
2	0.30	0.50	0.375	[39]	0.012
3	0.50	0.65	0.550	[28, 29]	0.006
4	0.65	0.90	0.825	[42]	0.001

Table 2 Name and X-ray temperature T_X of clusters in the four bins used in our analysis. Data in the first and second bins are from Ref. [38] and Ref. [39], respectively, while data for the third and fourth bins are from Ref. [28, 29] and Ref. [42], respectively. All errors are at the 68 % confidence level

bin i	name	T_X (keV)
1	A0754	$9.00^{+0.21}_{-0.21}$
	A2142	$8.46^{+0.32}_{-0.30}$
	COMA	$8.07^{+0.18}_{-0.16}$
	A2029	$7.93^{+0.24}_{-0.22}$
	A3266	$7.72^{+0.21}_{-0.17}$
	A0401	$7.19^{+0.17}_{-0.15}$
	A0478	$6.91^{+0.24}_{-0.22}$
	A2256	$6.83^{+0.14}_{-0.13}$
	A3571	$6.80^{+0.13}_{-0.11}$
	A0085	$6.51^{+0.10}_{-0.14}$
	A0399	$6.46^{+0.23}_{-0.22}$
	ZwCl1215	$6.36^{+1.79}_{-1.23}$
	A3667	$6.28^{+0.16}_{-0.16}$
	A1651	$6.22^{+0.27}_{-0.25}$
	A1795	$6.17^{+0.16}_{-0.15}$
	A2255	$5.92^{+0.24}_{-0.16}$
	A3391	$5.89^{+0.27}_{-0.20}$
	A2244	$5.77^{+0.37}_{-0.27}$
	A0119	$5.69^{+0.15}_{-0.17}$
	A1650	$5.68^{+0.18}_{-0.16}$
	A3395s	$5.55^{+0.54}_{-0.40}$
	A3158	$5.41^{+0.16}_{-0.15}$
	A2065	$5.37^{+0.21}_{-0.18}$
	A3558	$5.37^{+0.10}_{-0.09}$
	A3112	$4.72^{+0.23}_{-0.15}$
	A1644	$4.70^{+0.55}_{-0.43}$
2	MS 1008.1	$8.2^{+1.2}_{-1.1}$
	MS 1358.4	$6.9^{+0.5}_{-0.5}$
	MS 1621.5	$6.6^{+0.9}_{-0.8}$
	MS 0353.6	$6.5^{+1.0}_{-0.8}$
	MS 1426.4	$6.4^{+1.0}_{-1.2}$
	MS 1147.3	$6.0^{+1.0}_{-0.7}$
3	MS 0451–03	$10.4^{+0.7}_{-0.7}$
	MS 0016+16	$8.0^{+0.6}_{-0.6}$
4	MS 1054–03	$12.3^{+1.9}_{-1.3}$

Table 3 The threshold X-ray temperature, $T_{X,0}$, and the observed number of clusters with masses $M' > M'_0$, $\mathcal{N}'_{\mathrm{obs},i}$, in each bin and for each Δ'_v interval. The uncertainty on the comoving numbers of clusters, $\Delta\mathcal{N}'_{\mathrm{obs},i}$, is also indicated

	bin 1 $[T_{X,0}\ (\mathrm{keV}), \mathcal{N}'_{\mathrm{obs},1}]$	bin 2 $[T_{X,0}\ (\mathrm{keV}), \mathcal{N}'_{\mathrm{obs},2}]$	bin 3 $[T_{X,0}\ (\mathrm{keV}), \mathcal{N}'_{\mathrm{obs},3}]$	bin 4 $[T_{X,0}\ (\mathrm{keV}), \mathcal{N}'_{\mathrm{obs},4}]$
$\Delta'_v \in [25, 175]$	$[7.37, 5^{+1}_{-0}]$	$[9.6, 0^{+0}_{-0}]$	$[10.9, 0^{+1}_{-0}]$	$[12.8, 0^{+1}_{-0}]$
$\Delta'_v \in]175, 375]$	$[6.15, 15^{+2}_{-4}]$	$[8.1, 1^{+0}_{-1}]$	$[9.1, 1^{+1}_{-0}]$	$[10.7, 1^{+0}_{-0}]$
$\Delta'_v \in]375, 750]$	$[5.54, 21^{+2}_{-5}]$	$[7.3, 1^{+4}_{-1}]$	$[8.2, 2^{+0}_{-1}]$	$[9.6, 1^{+0}_{-0}]$
$\Delta'_v \in]750, 1750]$	$[5.14, 24^{+1}_{-1}]$	$[6.7, 2^{+4}_{-1}]$	$[7.6, 2^{+0}_{-1}]$	$[8.9, 1^{+0}_{-0}]$
$\Delta'_v \in]1750, 3250]$	$[4.91, 24^{+2}_{-0}]$	$[6.4, 5^{+1}_{-3}]$	$[7.3, 2^{+0}_{-0}]$	$[8.5, 1^{+0}_{-0}]$

The quantity Δ_v depends on redshift and cosmology and is thoroughly discussed in Appendix C.[5] As found in Ref. [43, 44], the parameter κ_Δ depends on Δ'_v and, in particular, when

$$\Delta'_v = 100, 250, 500, 1000, 2500, \tag{34}$$

κ_Δ assumes, respectively, the values

$$\kappa_\Delta = 0.76, 0.91, 1.01, 1.09, 1.14. \tag{35}$$

From Eq. (32), it follows that a mass M' within a comoving radius $R'_0 = 1.5h^{-1}$ Mpc is related to the X-ray temperature by

$$M' = 1.5 \times 10^{14} h^{-1} M_\odot \kappa_\Delta \frac{T_X}{\mathrm{keV}} \frac{1}{1+z}. \tag{36}$$

This means that clusters in the ith bin, with masses $M' > M_0$, will have a temperature exceeding the threshold value

$$\frac{T_{X,0}}{\mathrm{keV}} = \frac{16(1+z_c^{(i)})}{3\kappa_\Delta}. \tag{37}$$

In order to apply the above equation to data, we extrapolate the parameter κ_Δ according to the following prescription:

$$\kappa_\Delta = \begin{cases} 0.76 & \text{if } \Delta'_v \in [25, 175], \\ 0.91 & \text{if } \Delta'_v \in]175, 375], \\ 1.01 & \text{if } \Delta'_v \in]375, 750], \\ 1.09 & \text{if } \Delta'_v \in]750, 1750], \\ 1.14 & \text{if } \Delta'_v \in]1750, 3250]. \end{cases} \tag{38}$$

By using Eqs. (37) and (38) and data from Table 2 we find the values listed in Table 3 for the observed number of clusters with masses $M' > M'_0$ in the ith bin, $\mathcal{N}'_{\mathrm{obs},i}$.

The uncertainty in the comoving numbers of clusters, $\Delta\mathcal{N}'_{\mathrm{obs},i}$, derive from the uncertainty in the X-ray temperature of clusters. The threshold X-ray temperature in each bin and for each Δ'_v interval is also indicated in Table 3.

Finally, we calculate the observed number of clusters in the four redshift bins as

$$\mathcal{N}'_i = \alpha_i \int_{z_1^{(i)}}^{z_2^{(i)}} dz \frac{dV(z)}{dz} N'\big(M' > M'_0, z\big), \tag{39}$$

where we used Eq. (27) and replaced $\alpha(z)$ with the average effective fraction α_i in the ith bin. Since, as argued above, the α_i only depend weakly on the cosmology, we use in Eq. (39), for definiteness, the values for the case $\Omega_m = 0.3$ and $w = -1$ listed in Table 1.

In Fig. 1 we plot the various quantities needed in the computation of the mass function as a function of redshift and for different choices of (w_0, w_a). We fixed the values of the other cosmological parameters to the best-fit values obtained by using the 7-year WMAP observations [34], namely $(h, n, \Omega_m, \sigma_8) = (0.71, 0.96, 0.3, 0.80)$. Although the comoving volume is very sensitive to the choice of the cosmological model, the variations of the functions δ_c, $D(z)$, M_0/M'_0, and Δ_v (discussed in the appendices) with redshift and cosmology concur to give rise to larger changes in $N'(M' > M'_0, z)$, especially at large redshifts. This, in principle, can be used to put constraints on various models of dark energy.

Due to the small number of clusters in each bin, the comparison between observed and predicted number of clusters is made using Poisson error statistics. Accordingly, we define a likelihood function by

$$\mathcal{L} = \prod_{i=1}^{4} \frac{\lambda_i^{\kappa_i} e^{-\lambda_i}}{\kappa_i!}, \tag{40}$$

where we have introduced $\lambda_i \equiv \mathcal{N}'_i$ and $\kappa_i \equiv \mathcal{N}'_{\mathrm{obs},i}$ for notational clarity. The χ^2 statistics is then introduced as

$$\begin{aligned} &\chi^2_{\mathrm{CL,nosys}}(h, n, \Omega_m, \sigma_8, w_0, w_a) \\ &\quad = -2\ln\mathcal{L} \\ &\quad \simeq 2\sum_{i=1}^{4}\big[\mathcal{N}'_i - \mathcal{N}'_{\mathrm{obs},i}\big(1 + \ln\mathcal{N}'_i - \ln\mathcal{N}'_{\mathrm{obs},i}\big)\big]. \end{aligned} \tag{41}$$

[5] Defining r_Δ as the physical radius containing an overdensity of Δ'_v relative to the critical density, and $M(r < r_\Delta)$ as the mass contained in r_Δ, the mass–temperature relation (32) assumes the standard $T_X^{3/2}$ power-law form [43, 44], namely $M(r < r_\Delta) = \kappa_\Delta^{3/2}[3/4\pi\,\Delta'_v\rho_{\mathrm{cr}}^{(0)}]^{1/2}(1+z)^{-3/2}T_X^{3/2}$.

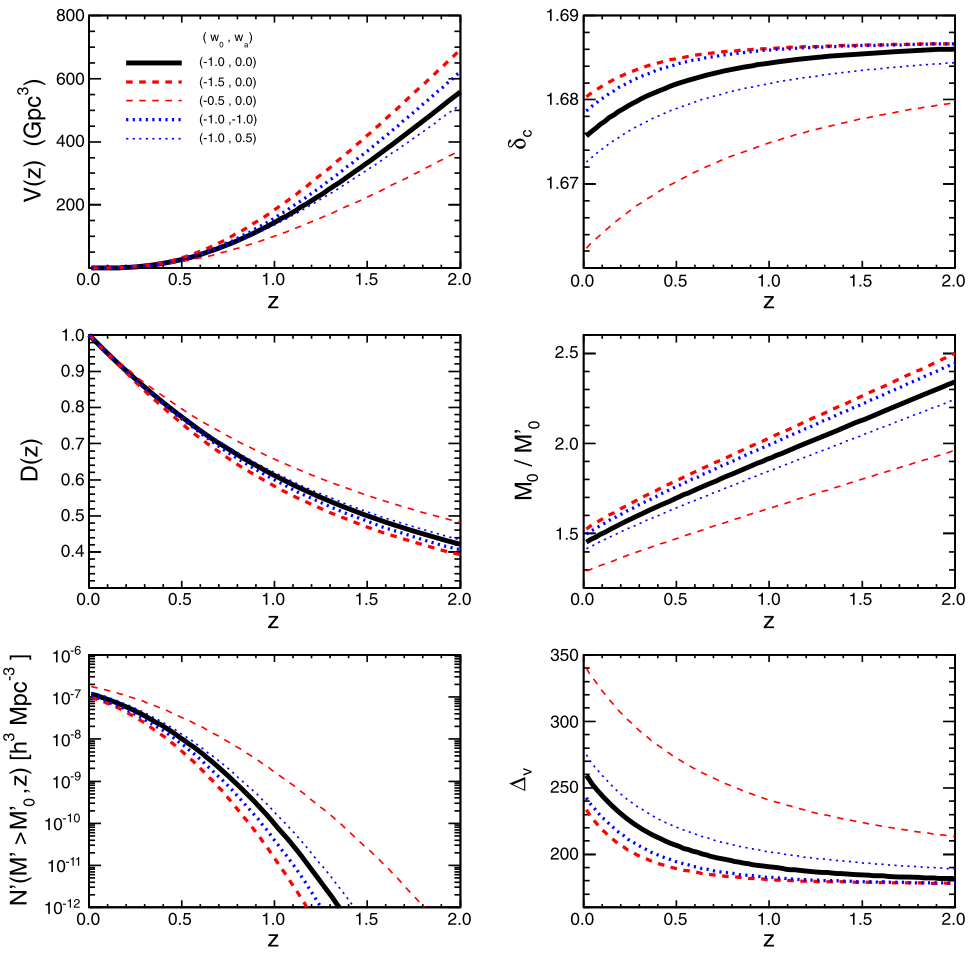

Fig. 1 The comoving volume $V(z)$, the critical density contrast $\delta_c(z)$, the growth factor $D(z)$, the mass ratio M_0/M_0', the mass function $N'(M' > M_0', z)$ [see Eq. (30)], and the virial overdensity relative to the background matter density, Δ_v, as a function of the redshift z, for different dark energy equation-of-state parameters (w_0, w_a). We fixed the values of the other cosmological parameters to $(h, n, \Omega_m, \sigma_8) = (0.71, 0.96, 0.3, 0.80)$

We also take into account the uncertainty in the comoving numbers of clusters, $\Delta\mathcal{N}'_{\mathrm{obs},i}$, by shifting the observed number of clusters in each bin as

$$\mathcal{N}'_{\mathrm{obs},i} \to \mathcal{N}'_{\mathrm{obs},i} + \xi\,\Delta\mathcal{N}'_{\mathrm{obs},i} \equiv \mathcal{N}''_{\mathrm{obs},i} \tag{42}$$

where the "pull" ξ is a univariate Gaussian random variable [46]. Correspondingly, we modify the χ^2 as

$$\chi^2_{\mathrm{CL}}(h, n, \Omega_m, \sigma_8, w_0, w_a, \xi) = 2\sum_{i=1}^{4}\left[\mathcal{N}'_i - \mathcal{N}''_{\mathrm{obs},i}\left(1 + \ln\mathcal{N}'_i - \ln\mathcal{N}''_{\mathrm{obs},i}\right)\right] + \xi^2. \tag{43}$$

3 Other cosmological data

In this section, we present data from other type of cosmological observations. In the next section, we derive joint constraints using these data along with those of massive clusters.

Baryon acoustic oscillations The measurement of baryon acoustic oscillations (BAOs) in the large-scale matter correlation function, fixes the values of a characteristic "BAO distance parameter", which we denote $\mathcal{C}$.[6]

With D_V an effective distance defined by

$$D_V(z) = \frac{1}{H_0}\left(\frac{z}{E(z)}\right)^{1/3}\left[\int_0^z \frac{dz'}{E(z')}\right]^{2/3}, \tag{44}$$

the $\mathcal{C}$ parameter is the ratio

$$\mathcal{C} = \frac{r_s(z_d)}{D_V(0.275)} \tag{45}$$

between the comoving sound horizon at the baryon drag epoch z_d,

$$r_s(z) = \frac{1}{\sqrt{3}H_0}\int_z^\infty \frac{dz'}{E(z')}\sqrt{\frac{4\Omega_\gamma(1+z)}{4\Omega_\gamma(1+z)+3\Omega_b}}, \tag{46}$$

and the effective distance D_V at $z = 0.275$ [50]. Here, Ω_γ is the photon density parameter that we take equal to $\Omega_\gamma h^2 =$

[6] See Refs. [47–49] for recent discussions of BAO data constraints on cosmological parameters.

2.56×10^{-5} [51].[7] For the redshift at the baryon drag epoch, z_d, we use the fitting formula of Ref. [37]:

$$z_d = \frac{1291(\Omega_m h^2)^{0.251}}{1+0.659(\Omega_m h^2)^{0.828}}\left[1+b_1\left(\Omega_b h^2\right)^{b_2}\right], \tag{47}$$

where

$$b_1 = 0.313\left(\Omega_m h^2\right)^{-0.419}\left[1+0.607\left(\Omega_m h^2\right)^{0.674}\right], \tag{48}$$

$$b_2 = 0.238\left(\Omega_m h^2\right)^{0.223}. \tag{49}$$

BAO data give the value $\mathcal{C}_{\rm obs} = 0.1390 \pm 0.0037$ [50]. Accordingly, we define the χ^2 statistic

$$\chi^2_{\rm BAO}(h, \Omega_m, w_0, w_a) = \frac{(\mathcal{C}-0.1390)^2}{0.0037^2}. \tag{50}$$

Cosmic microwave background The analysis of the CMB radiation puts a constraint on the reduced distance to the surface of last scattering, the so-called "CMB shift parameter",

$$\mathcal{R} = \Omega_m^{1/2}\int_0^{z_{\rm ls}} \frac{dz}{E(z)}, \tag{51}$$

where $z_{\rm ls} \simeq 1090$ is the redshift at the time of last scattering. The shift parameter weakly depends on the adopted cosmology and here we use the constraint found by Corasaniti and Melchiorri, $\mathcal{R}_{\rm obs} = 1.710 \pm 0.026$ [52], which refers to a cosmological model with evolving dark energy with equation-of-state parameter of the form given in Eq. (1). We then consider the following χ^2 statistic:

$$\chi^2_{\rm CMB}(\Omega_m, w_0, w_a) = \frac{(\mathcal{R}-1.710)^2}{0.026^2}. \tag{52}$$

Hubble constant A meta-analysis of many measurements yields $H_0 = (68 \pm 2.8)$ km/s/Mpc at 1σ C.L. [53, 54].[8] Accordingly, we introduce the penalty

$$\chi^2_h(h) = \frac{(h-0.68)^2}{0.028^2}. \tag{53}$$

Hubble parameter The analysis of spectra of passively evolving red galaxies enables the determination of the Hubble parameter at different redshifts, [57]. We use data quoted in Ref. [58] and reported in Table 4 for the sake of completeness. To these data we also add the estimate of the Hubble parameter at redshifts $z = 0.24$ and $z = 0.43$, obtained in Ref. [59] by using the BAO peak position as a standard ruler in the radial direction.[9]

Table 4 The observed Hubble parameter $H_{\rm obs}(z_i)$ with error σ_H (in brackets) from passively evolving galaxies (data from Ref. [58]) and line-of-sight BAO peak position (data are from Ref. [59] and marked with an asterisk)

z_i	$H_{\rm obs}(z_i)$ [km/s/Mpc]
0.1	69 (12)
0.17	83 (8)
0.24	79.69 (2.65)*
0.27	77 (14)
0.4	95 (17)
0.43	86.45 (3.68)*
0.48	97 (60)
0.88	90 (40)
0.9	117 (23)
1.3	168 (17)
1.43	177 (18)
1.53	140 (14)
1.75	202 (40)

We then introduce a χ^2 statistic as

$$\chi^2_{\rm Hubble}(h, \Omega_m, w_0, w_a) = \sum_{i=1}^{13}\frac{[H(z_i)-H_{\rm obs}(z_i)]^2}{\sigma_H^2}. \tag{54}$$

Type Ia supernovae Type Ia supernovae are standardizable candles and so can be used to discriminate between different cosmological models. Indeed, the theoretically predicted distance modulus μ, defined by

$$\mu(z) = 5\log_{10}\left(\frac{d_L}{1\ {\rm Mpc}}\right) + 25, \tag{55}$$

depends on the redshift and on the set of cosmological parameters (h, Ω_m, w_0, w_a) and can be compared to the one "derived" from the observation of SN lightcurves [66], namely μ_B. This, in turn, is deduced from the analysis of SN lightcurves which, if performed using the "SALT2" fitter [67], gives [66]

$$\mu_B = m_B^{\rm max} - M + \alpha x_1 - \beta c. \tag{56}$$

Here, $m_B^{\rm max}$ and c are the peak bolometric apparent magnitude and the color correction, respectively, while x_1 is a SALT2 fitter parameter [67]. The absolute magnitude of SNe, M, and α and β are, instead, nuisance parameters to be determined, simultaneously with the cosmological parameters from fits to data. In this paper, we use data from the Union2 SN compilation [66] which consists of 557 SNe.

[7] Since the upper limit of integration of the integral in Eq. (46) is infinity we must include, in the expression of the normalized Hubble parameter $E(z)$, the contribution due to radiation. Accordingly, we add the quantity $\rho_r/\rho_{\rm cr}^{(0)} = \Omega_r(1+z)^4$ in the argument of the square root appearing in Eq. (5), where ρ_r and Ω_r are the radiation energy density and radiation density parameter, respectively. We take $\Omega_r h^2 = 4.31 \times 10^{-5}$ [51].

[8] This is reasonably consistent with both 'low' [55] and 'high' [56] recent estimates of the Hubble constant.

[9] See Refs. [60–65] for Hubble parameter measurement constraints on cosmological parameters.

However, since the covariance matrices resulting from the lightcurve fit are not publicly available, we do not have any information on the correlation between the errors on $m_B^{\max}$, x_1, and c. Consequently, we follow the analysis of Refs. [52, 68] as explained in Ref. [69] and introduce the χ^2 statistic

$$\chi^2_{\rm SN}(\Omega_m, w_0, w_a) = \sum_{ij} \left(\mu_i^{\rm exp} - \tilde{\mu}_i\right)\left(\sigma_{ij}^{-2} - M_{ij}\right)\left(\mu_j^{\rm exp} - \tilde{\mu}_j\right). \quad (57)$$

The double sum runs over the 557 SNe, $\mu_i^{\rm exp}$ is the experimental value of the distance modulus of the ith supernova, and

$$\tilde{\mu}_i = 5\log_{10}\tilde{d}_L + 25, \quad (58)$$

is the "reduced" theoretical distance modulus. The "reduced" luminosity distance $\tilde{d}_L$ is

$$\tilde{d}_L = H_0 d_L, \quad (59)$$

and σ_{ij}^2 is the covariance matrix (containing both statistical and systematic errors), while the matrix M_{ij} is given by

$$M_{ij} = \frac{\sum_{kl}\sigma_{ik}^{-2}\sigma_{lj}^{-2}}{\sum_{kl}\sigma_{kl}^{-2}}. \quad (60)$$

It is worth noting that $\tilde{d}_L$ is independent of the Hubble parameter H_0, so the χ^2 in Eq. (57) depends only on the cosmological parameters (Ω_m, w_0, w_a).

There are many other data sets that can be used to constrain cosmological parameters, for example, strong gravitational lensing observations [70–73]; however, for our illustrative purposes here the data described above suffice.

4 Combined data analysis

In this section, we present the results of a joint analysis of massive cluster evolution, BAO peak length, CMB anisotropy, Hubble parameter, and SNe apparent magnitude data. The χ^2 statistic is

$$\chi^2(h, n, \Omega_m, \sigma_8, w_0, w_a, \xi) = \chi^2_{\rm CL} + \chi^2_{\rm BAO} + \chi^2_{\rm CMB} + \chi^2_h + \chi^2_{\rm Hubble} + \chi^2_{\rm SN}, \quad (61)$$

and depends on the six cosmological parameters $(h, n, \Omega_m, \sigma_8, w_0, w_a)$, and on the pull ξ.

Since the χ^2 depends on seven parameters, a grid-based analysis is not feasible and we therefore employ a Markov Chain Monte Carlo approach. We use a modified version of CosmoMC [68] to produce and analyze the likelihood chains.

4.1 (Ω_m, σ_8) results

In the left panel of Fig. 2, we show the results of the analysis in the (Ω_m, σ_8) plane for the cluster data alone. Here, we marginalize over the other parameters, using a flat prior, and determine the regions shown in the figure by finding where χ^2 increases by 1, 4, and 9, respectively, starting from the most likely set of values of the parameters. As a consequence of this convention [74], the projections of the allowed regions onto each parameter give, respectively, the 1σ, 2σ, and 3σ intervals for that parameter. The filled contours are obtained taking into account only statistical uncertainties (i.e., taking for $\mathcal{N}'_{{\rm obs},i}$ just the best-fit values listed in Table 3), while empty contours show the effect of including systematic errors on the comoving numbers of clusters.

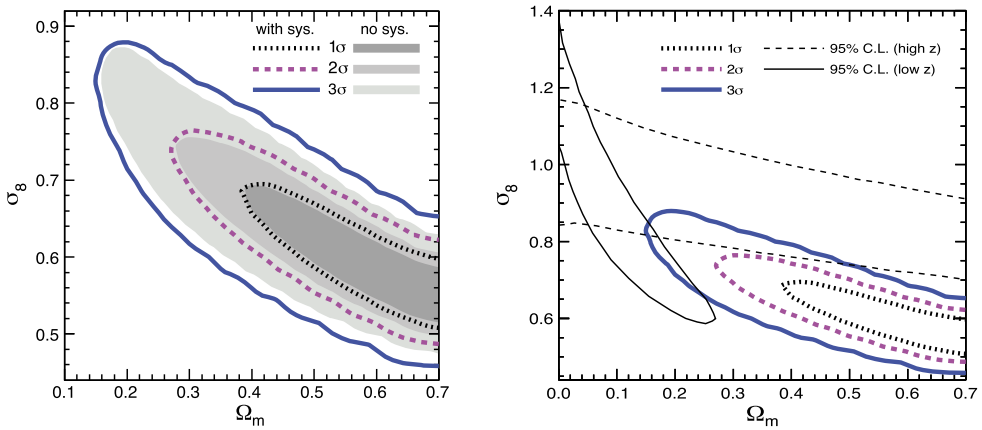

Fig. 2 *Left panel*. 1σ, 2σ, and 3σ confidence level contours in the (Ω_m, σ_8) plane from galaxy cluster number count data. Results obtained by including systematic uncertainties are shown as empty contours, while those ignoring systematics (i.e., keeping just best-fit values for data) are represented as filled contours. *Right panel*. Thick contours are the 1σ, 2σ, and 3σ ($\Delta\chi^2 = 1, 4, 9$) confidence level contours in the (Ω_m, σ_8) plane from galaxy cluster number count data (including systematic errors; the same as in the left panel). Thin continuous and thin dashed contours are the 95 % contour levels (2 d.o.f., $\Delta\chi^2 = 5.99$) for the first two redshift bins (low z) and last two redshift bins (high z), respectively, graphically reproduced from Refs. [28, 29]

As it is apparent, the differences between the two cases are marginal.

Cluster data prefer large values of Ω_m and low values of σ_8 with respect to the standard ΛCDM concordance model. Indeed, we find the marginalized bounds (including systematics),

$$\begin{aligned} &\Omega_m \geq 0.38 \quad (1\sigma \text{ C.L.}),\\ &\sigma_8 \leq 0.69 \quad (1\sigma \text{ C.L.}), \end{aligned} \tag{62}$$

in slight tension at 1σ with those obtained from the 7-year WMAP observations [34]: $\sigma_8 = 0.80 \pm 0.03$ (68 % C.L.) and $\Omega_m = 0.265 \pm 0.011$ (68 % C.L.), although compatible at 2σ confidence level. Note, however, that the WMAP's results are obtained assuming a spatially flat universe with cosmological constant and $H_0 = 71$ km/s/Mpc.

Our results on Ω_m and σ_8 can be also compared to other recent cosmological results coming from other galaxy cluster observations, obtained using different strategies and cluster surveys. In particular, studies of X-ray selected clusters, with masses exceeding a fixed mass threshold and distributed over fixed redshift ranges, yield lower values of Ω_m and larger values of σ_8, when compared with our limits (62). For example, Mantz et al. [19] find $\Omega_m = 0.23 \pm 0.04$ and $\sigma_8 = 0.82 \pm 0.05$ in a model with a constant dark energy. Conversely, the analysis of cluster population over low redshift ranges performed in [75] gives a result compatible with ours, namely $\Omega_m = 0.34^{+0.09}_{-0.08}$ and $\sigma_8 = 0.71^{+0.13}_{-0.16}$. Finally, the study of the evolution of the T_X-based mass function [20] within a model based on a cosmological constant, gives $\Omega_m = 0.34 \pm 0.08$, in good agreement with our result.

From our fit we derive the σ_8 normalization

$$\sigma_8 \Omega_m^{1/3} = 0.49 \pm 0.06 \quad (2\sigma \text{ C.L.}): \tag{63}$$

it is worth comparing our results with those of Refs. [28, 29], where the same set of cluster data was considered. In Refs. [28, 29], the authors analyze separately the data of the first two bins and the data of the last two bins, referring to low-redshift and high-redshift clusters, respectively (see Table 1). They find $\sigma_8 \Omega_m^{0.6} = 0.33 \pm 0.03$ from a fit to the data of the first two bins, and $\sigma_8 \Omega_m^{0.14} = 0.78 \pm 0.08$ from a fit to the data of the last two bins. The above results in the (Ω_m, σ_8) plane are shown in the right panel of Fig. 2, superimposed to our result. Requiring that both the above constraints be simultaneously satisfied, the authors in Refs. [28, 29] find $\Omega_m = 0.17 \pm 0.05$ (1σ C.L.) and $\sigma_8 = 0.98 \pm 0.10$ (1σ C.L.) for the allowed 1σ overlap region.

In conclusion, when our analysis is compared with that of Refs. [28, 29], it is seen that the two analysis agree only marginally, since our estimate favors relatively large values of Ω_m and low values of σ_8. We trace the differences to our proper treatment of cluster data, which depends on both redshift and cosmological parameters, and to the correct calculation of the mass function which takes into account the dependence of δ_c and Δ_v on redshift and cosmological parameters. Note that in Refs. [28, 29] the Hubble parameter and the spectral index are fixed (to the value $h = 0.72$ and $n = 1$) and $w = -1$. Also, the parameter κ_Δ in Eq. (32) is assumed to be cosmology-independent and the value used is simply the arithmetic mean of the values in Eq. (35), namely $\kappa_\Delta = 0.98$. The mass conversion is done by using the observed cluster profile in the comoving radius range $R \in [0.5, 2]h^{-1}$ Mpc. Since some of the clusters we use in the analysis have comoving radii exceeding the largest observed radius of $2h^{-1}$ Mpc, an extrapolation to higher value of R is performed by assuming a Navarro–Frenk–White profile for the virialized halo mass density (see Appendix B). Finally, the expressions for the critical density contrast, growth factor, virial overdensity, and virial radius refer, in Refs. [28, 29], to a matter dominated universe with $\Omega_m = 1$.

Figure 3 shows the results of the analysis in the (Ω_m, σ_8) plane when we combine the data on galaxy cluster count with all the other cosmological data, discussed in Sect. 3. Closed thick contours show the allowed region obtained combining cluster data (empty open thin contours) with all the remaining cosmological data (filled vertical bands), the latter independent of σ_8.

There is a slightly tension between the values of Ω_m preferred by the clusters and those preferred by the other cosmological probes, which are, however, compatible at 2σ level.

For the sake of completeness, we quote the 1σ confidence limits for (Ω_m, σ_8), derived from the joint analysis (clusters, BAO, CMB, Hubble parameter, and SNe):

$$\Omega_m = 0.28^{+0.03}_{-0.02} \quad (1\sigma \text{ C.L.}), \tag{64}$$

$$\sigma_8 = 0.73^{+0.03}_{-0.03} \quad (1\sigma \text{ C.L.}). \tag{65}$$

Let us conclude by giving the values of the minimum of the χ^2 for clusters alone, $\chi^2_{\text{CL,min}} = 0.54$, for the remaining cosmological data, $\chi^2_{\text{ALL}-\text{CL,min}} = 539.2$, and for the joint analysis, $\chi^2_{\text{ALL,min}} = 542.5$. Taking into account the numbers of degrees of freedom, of the same order of the values assumed by the χ^2 or slightly larger, these values confirm the goodness of our analysis.

4.2 (w_0, w_a) results

Figure 4 shows the result of our analysis in the (w_0, w_a) plane. Empty and filled contours in the left and right panels refer to the same cases as the left panel of Figs. 2 and 3, respectively.

It appears that current data on massive clusters do not allow one to appreciably constrain the equation-of-state parameters (w_0, w_a), to either favor or rule out a cosmological constant as dark energy (see left panel of Fig. 4).

The allowed 1σ confidence limits for (w_0, w_a), derived from the joint analysis (clusters, BAO, CMB, Hubble parameter, and SNe) are

$$w_0 = -1.14^{+0.14}_{-0.16} \quad (1\sigma \text{ C.L.}), \tag{66}$$

$$w_a = 0.85^{+0.42}_{-0.60} \quad (1\sigma \text{ C.L.}). \tag{67}$$

The joint analysis is compatible (at 2σ C.L.) with a cosmological constant as dark energy.

Moreover, we find

$$H_0 = 69.1^{+1.3}_{-1.5} \text{ km/s/Mpc} \quad (1\sigma \text{ C.L.}), \tag{68}$$

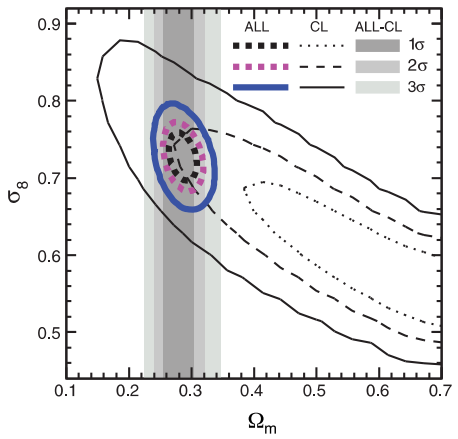

Fig. 3 1σ, 2σ, and 3σ confidence level contours in the (Ω_m, σ_8) plane from galaxy cluster number count (including systematic errors), BAO, CMB, Hubble parameter, and SNe observations. *Filled vertical bands* are the result of combining BAO, CMB, Hubble parameter, and SN data (ALL-CL), *empty open thin contours* give the confidence level contours for cluster data only (CL), while *empty closed thick contours* are from the combination of all data (ALL)

in agreement with a recent determination of the Hubble constant from the Hubble Space Telescope $H_0 = 73.8 \pm 2.4$ km/s/Mpc [76], and $\xi = -0.08^{+0.08}_{-0.90}$ (1σ C.L.).

The results of the global analysis are practically independent of n in the adopted range [0.90, 1.05].

For the sake of completeness, we report that from cluster data alone we find that the results of the fit are almost independent of n, that they are only very weakly dependent on h in the adopted range [0.6, 0.8], and that the pull is $\xi = -0.21^{+0.19}_{-0.74}$ (1σ C.L.).

4.3 XCDM results

Figure 5 shows the results of the analysis for the case $w_0 = w = \text{const}$ and $w_a = 0$ (the XCDM parametrization), in the (Ω_m, σ_8) and (Ω_m, w) planes.

Only clusters As in the case of general evolving dark energy with parameters (w_0, w_a), cluster data prefer large values of Ω_m, and relatively small values of σ_8,

$$\Omega_m \geq 0.43 \quad (1\sigma \text{ C.L.}), \tag{69}$$

$$\sigma_8 \leq 0.67 \quad (1\sigma \text{ C.L.}), \tag{70}$$

and put very weak bounds on w (see Fig. 5).

The left panel of Fig. 5 shows the correlation between Ω_m and σ_8 that can be approximatively parameterized by

$$\sigma_8 \Omega_m^{1/3} = 0.49 \pm 0.05 \quad (2\sigma \text{ C.L.}), \tag{71}$$

with a slightly smaller error on σ_8 with respect to Eq. (63).

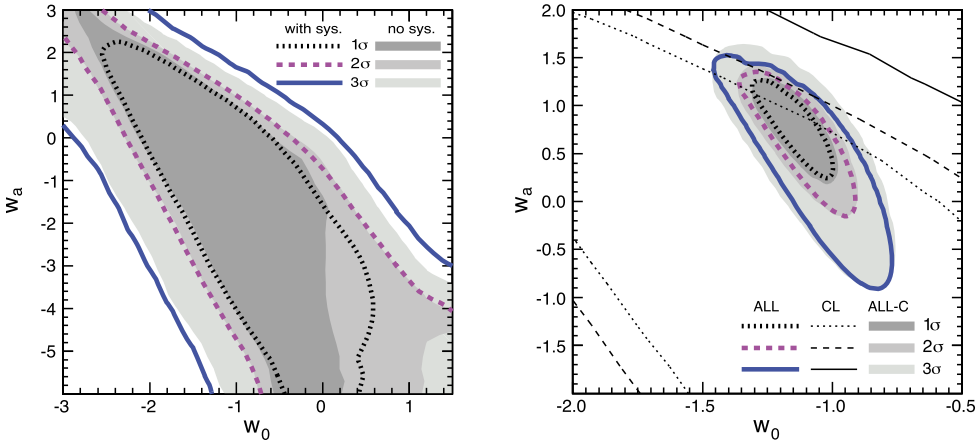

Fig. 4 1σ, 2σ, and 3σ confidence level contours in the (w_0, w_a) plane. *Left panel*. Results from galaxy cluster number count data obtained by including systematic uncertainties are shown as empty contours, while those ignoring systematics (i.e., keeping just best-fit values for data) are represented as *filled contours*. *Right panel*. Results determined from galaxy cluster number count (including systematic errors), BAO, CMB, Hubble parameter, and SNe observations. *Filled contours* are the result of combining BAO, CMB, Hubble parameter, and SN data (ALL-CL), *empty open thin contours* give the confidence level contours for cluster data only (CL), while *empty closed thick contours* are from the combination of all data (ALL)

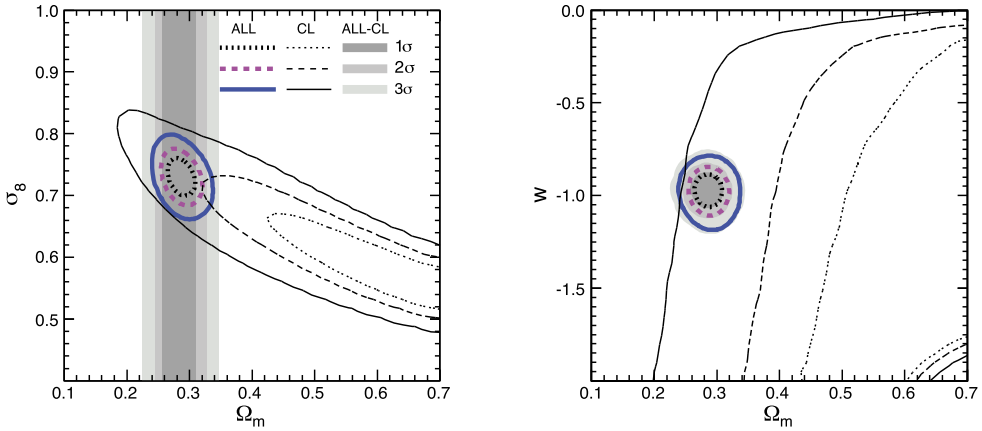

Fig. 5 1σ, 2σ, and 3σ confidence level contours in the (Ω_m, σ_8) plane (*left panel*) and in the (Ω_m, w) plane (*right panel*), for the XCDM parametrization, determined from galaxy cluster number count (including systematic errors), BAO, CMB, Hubble parameter, and SNe observations. *Filled contours* are the result of combining BAO, CMB, Hubble parameter, and SN data (ALL-CL), *empty open thin contours* give the confidence level contours for cluster data only (CL), while *empty closed thick contours* come from the combination of all data (ALL)

Combined data analysis The joint data analysis gives

$$\Omega_m = 0.28^{+0.03}_{-0.02} \quad (1\sigma \text{ C.L.}), \tag{72}$$

$$\sigma_8 = 0.73^{+0.03}_{-0.03} \quad (1\sigma \text{ C.L.}), \tag{73}$$

$$w = -0.96^{+0.08}_{-0.09} \quad (1\sigma \text{ C.L.}). \tag{74}$$

Also, we find

$$H_0 = 69.0^{+1.4}_{-1.4}\ \text{km/s/Mpc} \quad (1\sigma \text{ C.L.}), \tag{75}$$

and $\xi = -0.08^{+0.08}_{-0.90}$ (1σ C.L.). These results are almost independent of n.

Let us quoting, also in this case, the values of the minimum of the χ^2 for clusters alone, $\chi^2_{\text{CL,min}} = 0.56$, for the remaining cosmological data, $\chi^2_{\text{ALL-CL,min}} = 541.1$, and for the joint analysis, $\chi^2_{\text{ALL,min}} = 544.3$. As in the case of evolving dark energy, these values confirm the goodness of our fits.

Observational constraints on the XCDM parametrization have been derived from many different data sets, hence it provides a useful basis for comparing the discriminative power of different data. It is well known that SNeIa apparent magnitude versus redshift, BAO peak length scale, and CMB anisotropy data generally provide the most restrictive constraints on cosmological parameters. Clearly, currently available massive cluster evolution data is nowhere near as constraining as these data. However, cluster data results in constraints that are comparable to those that follow from angular size versus redshift data [77–81] and lookback time data [82–85], but are not as restrictive as those from galaxy cluster gas mass fraction measurements [86–88] or gamma-ray burst luminosity observations [89–92]. Over all, these constraints are approximately compatible with each other and with the ΛCDM model, lending support to the belief that we are converging on a standard cosmological model.

5 Dark energy models

The above analysis shows that the constraints on the equation of state of dark energy are only marginally affected by the inclusion of cluster data. Nevertheless, it is worth discussing the impact of these constraints on different dark energy models as in [93], since we include more cosmological probes and upgraded data with respect to the analysis in [93].

The advantage of the parametrization (1) of the dark energy equation of state is twofold: (i) a number of dark energy models can be adequately described by an equation of state of the form (1) at recent enough times (i.e., for a near unity); and, (ii) at a given redshift (such that $a \sim 1$) different classes of dark energy models correspond to different regions in the (w_0, w_a) plane [93]. Indeed, roughly speaking, there exist four classes of dark energy models: "thawing" models, "cooling" models, "barotropic" fluids (all assumed to obey the null energy condition $w \geq -1$), and "phantom" models (for which $w < -1$).[10] Introducing the quantity

$$w' = \frac{dw}{d\ln a}, \tag{76}$$

the classification is as follows.

Thawing models These satisfy the inequalities [94]

$$1 + w \lesssim w' \lesssim 3(1 + w), \tag{77}$$

and can arise in models of dark energy implemented by (cosmic) scalar fields, such as axions or dilatons, which roll

[10] This classification is not exhaustive since, as explained in [93], some models, such as those with oscillating equations of state, do not fall into it.

down towards the minimum of their potential. Typical potentials are of the form ϕ^m ($m > 0$), with ϕ being the scalar field. The bounds (77) are valid for $(1 + w) \ll 1$ so, following Ref. [94], we assume $w \lesssim -0.8$ as a practical limit of applicability. It should be noticed, as recently pointed out in Ref. [95], that is some scalar-field models, the thawing model parameter space is slightly larger than the one defined by Eq. (77).

Cooling models As for the case of thawing models, cooling models may arise in scalar-field models of dark energy. Typical scalar potentials are of the form ϕ^{-m} ($m > 0$). They lie in the region [94, 96]

$$-3(1 - w)(1 + w) < w' \lesssim \epsilon(z) w(1 + w), \tag{78}$$

where ϵ is a function of the redshift and an investigation of a variety of scalar-field cooling models indicates that $\epsilon(1) \simeq 0.2$ [94]. The upper bound in Eq. (78) is valid for $(1 + w) \ll 1$ [94] so, for this bound, we assume $w \lesssim -0.8$. Cooling models may arise in models of dynamical supersymmetry breaking and supergravity. So-called k-essence models [97] with a nonlinear kinetic term belong to this class [98].

Barotropic fluids These are fluids whose pressure p depends only on the energy density ρ. Assuming that $c_s^2 = dp/d\rho > 0$, barotropic fluids satisfy the inequality [96]

$$w' < 3w(1 + w), \tag{79}$$

and include (original [99] and generalized [100]) Chaplygin gas models.

Phantom models These are models which do not obey the null energy condition (see, however, Ref. [93]), and fall into the region

$$w < -1. \tag{80}$$

To each of the above models, we can associate a specific region in the (w_0, w_a) plane at a given reference time. Following Ref. [93], we take as reference time that corresponding to $z = 1$ which, roughly speaking, is when dark energy is expected to start to dominate over nonrelativistic matter. Phantom models at $z = 1$ can be split in two classes: "Pure phantom" models which did not cross the phantom divide line $w = -1$ recently,

$$w_0 < -1, \qquad w(z = 1) < -1, \tag{81}$$

and models that crossed $w = -1$ from a lower value to a higher value,

$$w_0 > -1, \qquad w(z = 1) < -1, \tag{82}$$

which we dub "bottom-up phantom" models.

Finally, we also consider models that crossed $w = -1$ from a higher value to a lower value:

$$w_0 < -1, \qquad w(z = 1) > -1. \tag{83}$$

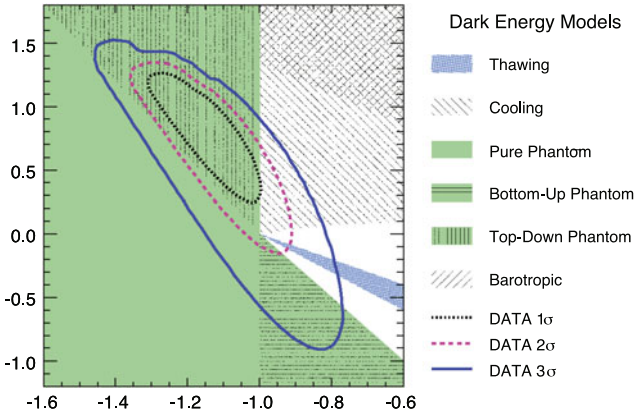

Fig. 6 1σ, 2σ, and 3σ confidence level contours in the (w_0, w_a) plane from the joint analysis of galaxy cluster number count (with systematics), BAO, CMB, Hubble parameter, and SNe (the same as in the right panel of Fig. 4). The *shaded areas* represent different types of evolving dark energy model according to the classification of Ref. [93]

These models, which we dub "top-down phantom" models, are phantom today ($z = 0$) and non-phantom at $z = 1$.

The (w_0, w_a) plane containing all the above regions is presented in Fig. 6, together with the regions allowed by data and discussed in Sect. 5.[11]

Figure 6 shows the 1σ, 2σ, and 3σ confidence level contours in the (w_0, w_a) plane (obtained from the global analysis) superimposed on the regions representing different types of evolving dark energy model according to the classification of Ref. [93]. At the 1σ level, phantom models of evolving dark energy of top-down type are slightly favored over cooling models and considerably preferred over thawing, pure, and bottom-up phantom models. Non-phantom barotropic fluids are ruled out.

6 Conclusions

We have constrained cosmological parameters by using X-ray temperature data of massive galaxy clusters in the redshift range $0.05 \lesssim z \lesssim 0.83$ with masses within a comoving radius of $1.5h^{-1}$ Mpc greater than the fiducial value $8 \times 10^{14} h^{-1} M_\odot$.

In this analysis, we have accounted for the dependence of quantities related to cluster physics—such as the critical density contrast, the growth factor, the mass conversion factor, the virial overdensity, and the virial radius—on the

[11] There are a few disadvantages of the parametrization of Eq. (1): (i) This two parameter (w_0, w_a) parametrization has one more parameter than the simplest consistent and physically motivated scalar-field dark energy model [16, 17], thus making it more difficult to constrain model parameters with observational data; and, (ii) even so, the parametrization is not physically complete as additional information must be provided if one is interested in the evolution of energy density and other spatial inhomogeneities [101, 102].

cosmological model parameters $\Omega_m, \sigma_8, n, w_0, w_a$, and H_0. We have also taken into account the dependence on redshift and cosmological parameters of the mass–temperature relation which allow us to convert the observed cluster X-ray temperatures into cluster masses and to calculate the cluster number counts.

The analyses show that cluster data prefer small values of the amplitude of mass fluctuations σ_8,

$$\textit{only clusters:} \quad \sigma_8 \leq 0.69 \quad (1\sigma \text{ C.L.}), \tag{84}$$

as well as large values of nonrelativistic matter energy density,

$$\textit{only clusters:} \quad \Omega_m \geq 0.38 \quad (1\sigma \text{ C.L.}). \tag{85}$$

The above bounds are in slight tension at 1σ with those obtained from the 7-year WMAP observations, although compatible at 2σ confidence level. In addition, we have found the following normalization of σ_8:

$$\textit{only clusters:} \quad \sigma_8 \Omega_m^{1/3} = 0.49 \pm 0.06 \quad (2\sigma \text{ C.L.}). \tag{86}$$

We have found that currently available cluster data do not tightly constrain the dark energy equation of state, and that a cosmological constant is consistent with these observations.

Cluster data alone are not sensitive to the value of the index n of the power-law power spectrum of the density perturbations, and are only very weakly dependent on the Hubble constant H_0.

In order to break the Ω_m–σ_8 degeneracy and put more stringent constraints on cosmological parameters, we have combined cluster data with BAO peak length scale observations, CMB anisotropy data, Hubble constant and Hubble parameter measurements, and type Ia supernova magnitude–redshift observations. In this case we find

$$\textit{all data:} \quad \sigma_8 = 0.73^{+0.03}_{-0.03} \quad (1\sigma \text{ C.L.}) \tag{87}$$

and

$$\textit{all data:} \quad \Omega_m = 0.28^{+0.03}_{-0.02} \quad (1\sigma \text{ C.L.}), \tag{88}$$

which are in good agreement with previous constraints in the literature (such as those coming from WMAP).

Regarding the equation-of-state parameters of dark energy, we find

$$\textit{all data:} \quad w_0 = -1.14^{+0.14}_{-0.16}, \qquad w_a = 0.85^{+0.42}_{-0.60} \quad (1\sigma \text{ C.L.}), \tag{89}$$

which indicates that the joint analysis is consistent with a cosmological constant. Moreover, the combination of all data is almost insensitive to n, and constrains the Hubble parameter to the range,

$$\textit{all data:} \quad H_0 = 69.1^{+1.3}_{-1.5}\ \text{km/s/Mpc} \quad (1\sigma \text{ C.L.}), \tag{90}$$

consistent with recent bounds from Hubble Space Telescope observations.

Similar results are found in the case of constant equation-of-state parameter time-varying dark energy (the XCDM parametrization).

Our results suggest that, among models of dark energy with varying equation of state (i.e., with $w_a \neq 0$), the top-down phantom models, for which the equation of state crossed the phantom divide line from a higher value to a lower value, are preferred over non-phantom thawing and cooling models. Finally, non-phantom barotropic fluids are excluded as models of dark energy.

While currently available massive cluster data do not constrain cosmological parameters as tightly as do SNeIa apparent magnitude versus redshift measurements, or CMB anisotropy data, or BAO peak length scale observations, the cluster measurements do provide constraints comparable to those from some of the other available data sets. They also play a useful role in constraining cosmological parameters when used in conjunction with other data. More importantly, we look forward to superior quality near-future massive cluster data, and anticipate the significantly more restrictive parameter constraints that will result from using the techniques we have developed here.

Acknowledgements We would like to thank A. Natarajan for useful comments. T.K. acknowledges partial support from Georgian National Science Foundation grant ST08/4-422, Swiss National Science Foundation SCOPES grant 128040, NASA grant NNXlOAC85G, NSF grant AST-1109180, the ICTP associate membership program, and the Università Degli Studi Di Bari for hospitality. B.R. acknowledges support from DOE grant DEFG03-99EP41093 and NSF grant AST-1109275.

Appendix A: Critical density contrast and growth factor

Critical density contrast The critical density contrast δ_c depends on the redshift and on the cosmology and can be evaluated, using the approach of Ref. [103] (see also Ref. [104]), as follows. Consider the full nonlinear equation describing the evolution of the density contrast:

$$\delta'' + \left(\frac{3}{a} + \frac{E'}{E}\right)\delta' - \frac{4}{3}\frac{\delta'^2}{1+\delta} - \frac{3}{2}\frac{\Omega_m}{a^5 E^2}\delta(1+\delta) = 0, \tag{A.1}$$

where a prime indicates differentiation with respect to the scale factor a and

$$\delta = \frac{\delta\rho_m}{\rho_m} = \frac{\rho_{\text{cluster}} - \rho_m}{\rho_m} \tag{A.2}$$

is the density contrast with ρ_{cluster} being the cluster matter density. Since the above equation describes the nonlinear growth of the density contrast, its value at some chosen collapse time t_{collapse} diverges. The critical density contrast δ_c at the time t_{collapse} is, by definition, the value of the density contrast at the time t_{collapse} obtained by solving the linearized version of Eq. (A.1), namely

$$\delta'' + \left(\frac{3}{a} + \frac{E'}{E}\right)\delta' - \frac{3}{2}\frac{\Omega_m}{a^5 E^2}\delta = 0, \tag{A.3}$$

with boundary conditions for δ such that the same boundary conditions applied to the nonlinear equation (A.1) make δ divergent at $t_{\rm collapse}$. Following Ref. [103], we take for the initial derivative of δ, $\delta'(a_i)$, the value $\delta'(a_i) = 5 \times 10^{-5}$ where $a_i \equiv 5 \times 10^{-5}$, while the initial value of the density contrast, $\delta(a_i)$, is found by searching for the value of $\delta(a_i)$ such that δ diverges at the time $t_{\rm collapse}$. We assume (as in Ref. [103]) that the divergency is achieved, numerically, when δ exceeds the value 10^7.

In Fig. 1, we plot the critical density contrast, δ_c, as a function of the redshift for different values of (w_0, w_a). For large redshifts—where the effects of dark energy become negligible compared to those of nonrelativistic matter—the Universe effectively approaches the Einstein–de Sitter model where the critical density contrast is independent of the redshift and is $\delta_c = (3/20)(12\pi)^{2/3} \simeq 1.686$ [3]. In Fig. 7, we show the δ_c-isocontours in the (w_0, w_a)-plane for different values of the redshift and for $\Omega_m = 0.27$.

Growth factor The z-dependent part of the matter power spectrum—the growth factor $D(z)$—is

$$D(z) = \frac{\delta(z)}{\delta(0)}, \tag{A.4}$$

and satisfies the linearized equation (A.3). The boundary conditions we impose are $D(a = 1) = 1$ and $D(a = a_i) = a_i$, where, as before, $a_i \equiv 5 \times 10^{-5}$. In Fig. 1 we plot the growth factor, $D(z)$, as a function of the redshift for different values of (w_0, w_a).

Appendix B: Mass conversion

The virial mass in the PS or ST parametrization needs to be expressed as a function of the observed mass M' within a reference comoving radius of $R'_0 = 1.5h^{-1}$ Mpc. As described in Sect. 2.2, what we really need is the fiducial virial mass M_0 as a function of the fiducial mass within R'_0

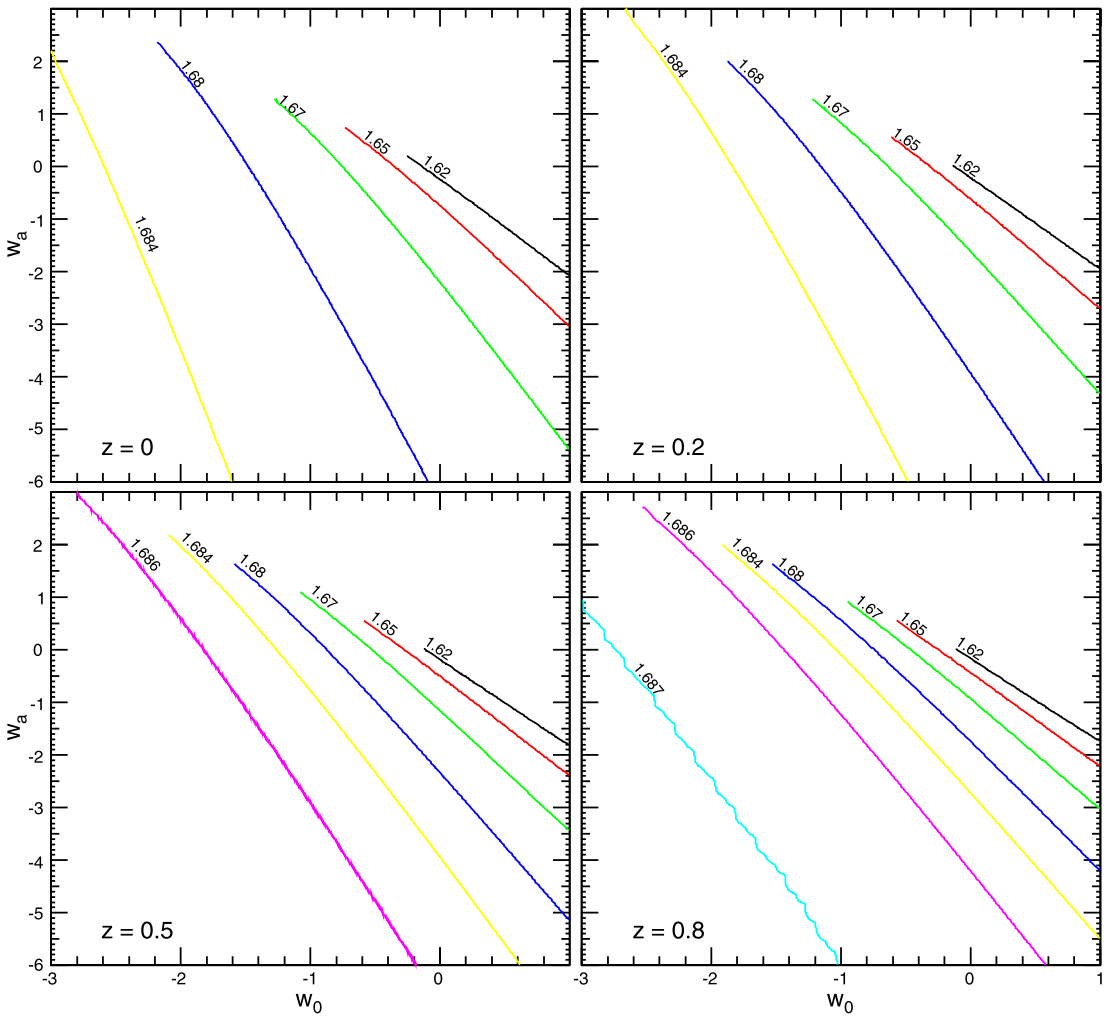

Fig. 7 δ_c-isocontours in the (w_0, w_a)-plane for different values of the redshift and for $\Omega_m = 0.27$

adopted in the observation, namely $M_0' = 8 \times 10^{14} h^{-1} M_\odot$. We use the following procedure to accomplish this. We first determine the physical virial radius $r_{v,0}$, within which the virial mass M_0 is contained, through the relation

$$M_0(z) = \frac{4\pi}{3} r_{v,0}^3(z) \rho_m(z) \Delta_v(z) = \frac{4\pi}{3} R_{v,0}^3 \rho_m^{(0)} \Delta_v(z), \quad \text{(B.1)}$$

where $R_{v,0} = (1+z) r_{v,0}$, and Δ_v is the virial overdensity and is discussed in Appendix C. We then scale the virial mass M_0 to the $1.5h^{-1}$ Mpc comoving radius assuming a Navarro–Frenk–White profile for the virialized halo mass density [105]:

$$\rho_{\rm cluster}(r) = \frac{4\rho_{\rm cluster}(r_s)}{(r/r_s)(1+r/r_s)^2}, \quad \text{(B.2)}$$

where r is the physical radial distance and r_s is a physical scale radius.

Technically the procedure is as follows. From Eq. (B.2) we can obtain the mass $M(<r)$ contained in the physical radius r:

$$\begin{aligned} M(<r) &= 4\pi \int_0^r dr' r'^2 \rho_{\rm cluster}(r') \\ &= 16\pi \rho_{\rm cluster}(r_s) r^3 f(r_s/r), \end{aligned} \quad \text{(B.3)}$$

where

$$f(x) = x^3 \left[\ln\left(\frac{1+x}{x}\right) - \frac{1}{1+x} \right]. \quad \text{(B.4)}$$

Then applying Eq. (B.3) to the mass M_0 within the physical virial radius $r_{v,0}$, and to the mass M_0' within the physical radius $r_0' = R_0'/(1+z)$ corresponding to the comoving radius R_0', and taking the ratio of these two equations, we get

$$\frac{M_0}{M_0'} = \left(\frac{R_{v,0}}{R_0'}\right)^3 \frac{f(1/c_{v,0})}{f(R_{v,0}/c_{v,0}R_0')}. \quad \text{(B.5)}$$

Here

$$c_{v,0} = \frac{r_{v,0}}{r_s} \quad \text{(B.6)}$$

is the "concentration parameter"

$$c_v = \frac{r_v}{r_s} \quad \text{(B.7)}$$

—the ratio between the physical virial radius r_v and the physical scale radius r_s—evaluated at the physical virial radius $r_{v,0}$.

Both $R_{v,0}$ and $c_{v,0}$ in Eq. (B.5) are functions of M_0. From Eq. (B.1) we can express $R_{v,0}$ as a function of M_0. For $c_{v,0}$, we proceed as follows. First we consider the expression for the concentration parameter found by Bullock et al. [106] in their N-body simulation:

$$c_v(M_v) = \frac{B}{1+z} \left[\frac{M_v(0)}{M_*(0)} \right]^{-\beta}. \quad \text{(B.8)}$$

Here $B \simeq 9$, $\beta \simeq 0.13$,[12] M_v is the mass within a physical virial radius r_v,

$$M_v(z) = \frac{4\pi}{3} r_v^3(z) \rho_m(z) \Delta_v(z), \quad \text{(B.9)}$$

and $M_*(z)$ is a fiducial mass defined by

$$\sigma\big(R_*(z), z\big) = \delta_c(z), \quad \text{(B.10)}$$

where the comoving radius $R_*(z)$ is defined by

$$M_*(z) = \frac{4\pi}{3} R_*^3(z) \rho_m^{(0)}. \quad \text{(B.11)}$$

Then, evaluating Eq. (B.8) for $M_v = M_0$ [which corresponds to evaluating Eq. (B.7) for $r_v = r_{v,0}$], we have

$$c_{v,0} = c_v(M_0) = \frac{c_{v,0}'}{\gamma} \left(\frac{M_0}{M_0'} \right)^{-\beta}, \quad \text{(B.12)}$$

where

$$c_{v,0}' = c_v\big(M_0'\big) = \frac{B}{1+z} \left[\frac{M_0'}{M_*(0)} \right]^{-\beta} \quad \text{(B.13)}$$

is, formally, the concentration parameter (B.8) evaluated at M_0' [see Eq. (B.8)], and

$$\gamma(z) = \left[\frac{\Delta_v(z)}{\Delta_v(0)} \right]^{-\beta}. \quad \text{(B.14)}$$

Taking into account Eqs. (22), (24), and (B.10), we find that the quantity $M_*(0)$ does not depend on M_0 and is defined by

$$\Sigma\big(R_*(0)/R_0\big) = \frac{\delta_c(0)}{\sigma_8}. \quad \text{(B.15)}$$

Finally, inserting Eqs. (B.1) and (B.12) in Eq. (B.5), we obtain the equation that gives M_0 as a function of M_0' [namely the equation defining the function g in Eq. (31)]:

$$f\left(R_{1.5} \frac{\gamma}{c_{v,0}'} \left(\frac{M_0}{M_0'} \right)^{\beta+1/3} \right) = R_{1.5}^3 f\left(\frac{\gamma}{c_{v,0}'} \left(\frac{M_0}{M_0'} \right)^{\beta} \right), \quad \text{(B.16)}$$

where

$$R_{1.5}(z) = \frac{[3M_0'/4\pi\rho_m^{(0)}\Delta_v(z)]^{1/3}}{1.5h^{-1}\ \text{Mpc}} \quad \text{(B.17)}$$

is the comoving virial radius corresponding to the mass M_0', normalized to $1.5h^{-1}$ Mpc.

In a flat universe dominated by nonrelativistic matter (the Einstein–de Sitter model), the comoving virial radius corresponding to the mass $M_0' = 8 \times 10^{14} h^{-1} M_\odot$ is about $1.57h^{-1}$ Mpc, which gives $R_{1.5} \simeq 1$. This in turn means, using Eq. (B.16), that $M_0/M_0' \simeq 1$, namely the virial mass contained in a sphere of comoving virial radius of $1.5h^{-1}$ Mpc is approximatively M_0'. Due to the presence of the third root in Eq. (B.17), the function $R_{1.5}(z)$ is fairly insensitive to

[12] To be precise, B and β can (weakly) depend on the cosmology and the values used here are those found in Ref. [106] where a cosmology with cosmological constant was assumed.

changes in the adopted cosmology [through $\rho_m^{(0)}$ and $\Delta_v(z)$]. Therefore, also in the case of a generic cosmology with evolving dark energy, we expect values of M_0 close to M_0'.

In Fig. 1, we plot the ratio M_0/M_0' as a function of the redshift for different values of (w_0, w_a). M_0, as argued, turns to be of order (of a few times) M_0'.

Appendix C: Virial overdensity and virial radius

Virial overdensity The virial overdensity is the ratio of the cluster mass density and the background matter density at the time of virialization:

$$\Delta_v(z=z_v) = \frac{\rho_{\rm cluster}(z_v)}{\rho_m(z_v)}, \tag{C.1}$$

where z_v is the redshift at the time of virialization.

Using the fact that the cluster mass density is

$$\rho_{\rm cluster}(z) = \frac{3M_{\rm cluster}}{4\pi r^3(z)}, \tag{C.2}$$

where $M_{\rm cluster}$ is the halo cluster mass and $r(z)$ the physical halo radius, we can rewrite Eq. (C.1) as

$$\Delta_v(z=z_v) = \left(\frac{r_{\rm ta}}{r_v}\right)^3 \left(\frac{1+z_{\rm ta}}{1+z_v}\right)^3 \zeta, \tag{C.3}$$

where $r_{\rm ta}$ and r_v are, respectively, the physical radii of the halo cluster at turn-around and at virialization (r_v is, in other words, the physical virial radius of the halo cluster), while $z_{\rm ta}$ and

$$\zeta = \frac{\rho_{\rm cluster}(z_{\rm ta})}{\rho_m(z_{\rm ta})} \tag{C.4}$$

are, respectively, the redshift and virial overdensity at the time of turn-around.

The redshift at the virialization time is

$$z_v = z_{\rm collapse}, \tag{C.5}$$

and follows from the standard assumption that clusters virialize at the time of collapse.

To find the redshift at the time of turn-around, $z_{\rm ta}$, and to obtain the virial overdensity at the turn-around time, ζ, we follow the procedure of Ref. [103]. First, they observed that the quantity $(\delta+1)/a^3$, where δ is the density contrast that satisfies the nonlinear Eq. (A.1), is proportional to $1/r^3(z)$:

$$\frac{\delta+1}{a^3} = \frac{3M_{\rm cluster}}{4\pi\rho_m^{(0)}}\frac{1}{r^3(z)}, \tag{C.6}$$

where $r(z)$ is the collapsing sphere's radius. [It is straightforward to get the above equation by using Eqs. (A.2) and (C.2).] Then since $r(z)$ assumes the maximum value at the turn-around time, the time of turn-around is found by minimizing the quantity $(\delta+1)/a^3$, where δ is the solution of Eq. (A.1) obtained by imposing the boundary conditions used in Appendix A.

Once the turn-around time is found, the virial overdensity at the turn-around time is simply given, from Eqs. (A.2) and (C.4), by

$$\zeta = \delta(z_{\rm ta}) + 1, \tag{C.7}$$

where δ is the solution of Eq. (A.1).

The ratio of the virial radius to the turn-around radius, $r_v/r_{\rm ta}$, as a function of cosmological parameters is analyzed below.

In Fig. 1 we plot the virial overdensity at the time of virialization, Δ_v, as a function of the redshift for different values of (w_0, w_a). In an Einstein–de Sitter model (i.e., for $\Omega_m = 1$), the standard assumption that $t(z_v) \simeq 2t(z_{\rm ta})$ together with the fact that $r_v = r_{\rm ta}/2$ and $\zeta = (3\pi/4)^2$, gives $\Delta_v \simeq 18\pi^2 \simeq 177.653$ (independent of the redshift). Indeed, each curve in Fig. 1 approaches this value for a sufficiently large value of the redshift since, as already noted, the Universe then enters the Einstein–de Sitter regime where the effects of dark energy become subdominant with respect to those of nonrelativistic matter.

In Fig. 8, we show the Δ_v-isocontours in the (w_0, w_a)-plane for different values of the redshift and for $\Omega_m = 0.27$.

Virial radius In order to "estimate" the quantity $r_v/r_{\rm ta}$, we apply energy conservation and the virial theorem to the spherical collapse of the cluster halo.

We start by considering the total gravitational potential energy $U(r)$ of a sphere of radius r containing the cluster mass $M_{\rm cluster}$ and dark energy:

$$U(r,z) = U_{mm}(r) + U_{m\rm DE}(r,z), \tag{C.8}$$

where

$$U_{mm}(r) = -\frac{3}{5}\frac{GM_{\rm cluster}^2}{r} \tag{C.9}$$

is the familiar gravitational potential self-energy of a sphere of nonrelativistic matter, and

$$U_{m\rm DE}(r,z) = -\frac{4\pi}{5}GM_{\rm cluster}\big[1+3w(z)\big]\rho_{\rm DE}(z)r^2 \tag{C.10}$$

is the gravitational potential energy of interaction between nonrelativistic matter and dark energy.[13]

Since the potential energy $U_{m\rm DE}(r,z)$ depends explicitly on the time, the system under consideration is not conservative. Therefore, neither energy conservation nor the virial theorem can be applied.[14]

[13] Here, we are considering the case where the dark energy does not cluster and does not virialize, so that the only terms in the potential energy which are relevant for energy conservation and virialization are those in Eq. (C.8) [107].

[14] It is straightforward to show that the only case where $U_{m\rm DE}(r,z)$ is z-independent, and the system is conservative, is that of the cosmological constant, namely $w(z) = -1$ for all times.

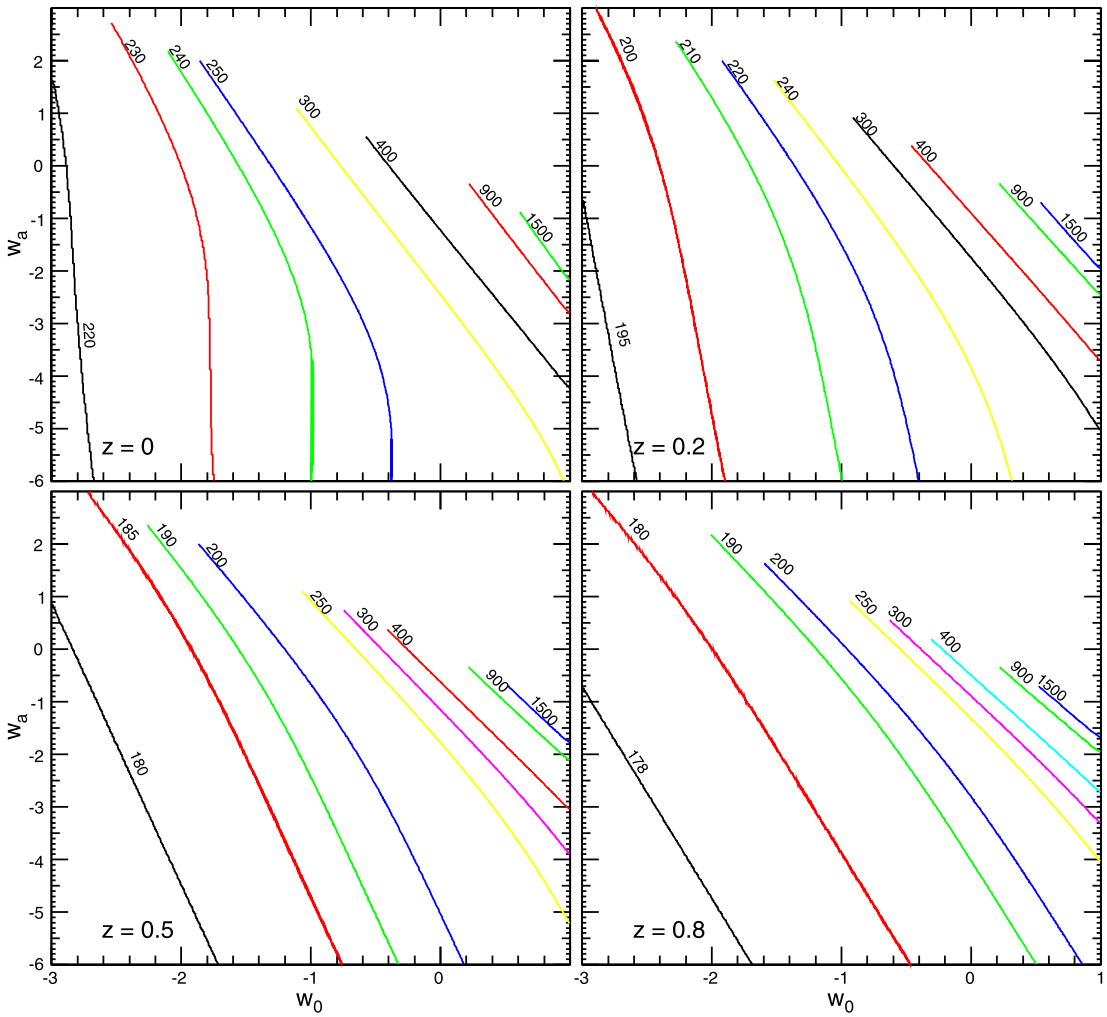

Fig. 8 Δ_v-isocontours in the (w_0, w_a)-plane for different values of the redshift. We fixed $\Omega_m = 0.27$

In order to get a conservative system, Wang [107] has suggested replacing the z-dependent quantity $[1 + 3w(z)]\rho_{\rm DE}(z)$ with the same quantity evaluated at the turn-around time.

Here we propose defining an effective potential energy, which does not depend explicitly on the time, as

$$U^{(\rm eff)}(r) = U_{mm}(r) + U^{(\rm eff)}_{m\rm DE}(r), \tag{C.11}$$

where

$$U^{(\rm eff)}_{m\rm DE}(r) = -\frac{4\pi}{5} G M_{\rm cluster} \big\langle \big[1 + 3w(z)\big]\rho_{\rm DE}(z) \big\rangle r^2 \tag{C.12}$$

is the effective potential energy of interaction and $\langle \ldots \rangle$ is an operator that when applied to a z-dependent function $\psi(z)$ gives a z-independent quantity, i.e.

$$\frac{d\langle \psi(z)\rangle}{dz} = 0. \tag{C.13}$$

The action of the $\langle \ldots \rangle$-operator is specified below.

The introduction of the effective energy potentials (C.11) and (C.12), allow us to use the energy conservation theorem that, applied at the times of virialization and turn-around, gives

$$\mathcal{K}(r_v) + U^{(\rm eff)}(r_v) = U^{(\rm eff)}(r_{\rm ta}), \tag{C.14}$$

where $\mathcal{K}(r_v)$ is the kinetic energy at the virialization time.

Using the virial theorem

$$\mathcal{K}(r_v) = \left(\frac{r}{2} \frac{dU^{(\rm eff)}(r)}{dr} \right)_{r=r_v}, \tag{C.15}$$

the energy conservation equation (C.14) takes the form

$$\frac{1}{2} U_{mm}(r_v) + 2U^{(\rm eff)}_{m\rm DE}(r_v) = U_{mm}(r_{\rm ta}) + U^{(\rm eff)}_{m\rm DE}(r_{\rm ta}). \tag{C.16}$$

Taking into account Eqs. (C.2) and (C.4), the mass of the cluster is

$$M_{\rm cluster} = \frac{4\pi}{3} r^3_{\rm ta} \rho_m(z_{\rm ta}) \zeta, \tag{C.17}$$

so that Eq. (C.16) reads

$$4\eta q(1+3w_{\rm ta})\left(\frac{r_v}{r_{\rm ta}}\right)^3 - 2\big[1+\eta q(1+3w_{\rm ta})\big]\left(\frac{r_v}{r_{\rm ta}}\right)+1 = 0. \tag{C.18}$$

Here $w_{\rm ta} = w(z_{\rm ta})$ and we have defined, following [107], the quantity

$$q = \frac{\rho_{\rm DE}(z_{\rm ta})}{\zeta\rho_m(z_{\rm ta})}. \tag{C.19}$$

We have also introduced the "deviation parameter", η, as

$$\eta = \frac{\langle[1+3w(z)]\rho_{\rm DE}(z)\rangle}{(1+3w_{\rm ta})\rho_{\rm DE}(z_{\rm ta})}. \tag{C.20}$$

It is worth noting that in the case of a cosmological constant the system is conservative (see footnote 14), and the equation determining $r_v/r_{\rm ta}$ is formally given by Eq. (C.18) with $\eta = 1$. Hence, the only restriction to the action of the $\langle\ldots\rangle$-operator is that, when applied to the function $[1+3w(z)]\rho_{\rm DE}(z)$, it must give $\eta = 1$ for $w(z) = -1$.

Taking $\langle\psi(z)\rangle = \psi(z_{\rm ta})$ corresponds to the choice of Wang, which also implies $\eta = 1$ for equation-of-state parameter $w(z)$. However, taking $\langle\psi(z)\rangle = \psi(\bar{z})$, where $\bar{z}$ can be anywhere in the interval $[z_v, z_{\rm ta}]$, is also a plausible choice.

In the upper panel of Fig. 9, we plot the ratio of the virial radius to the turn-around radius in the case $\eta = 1$ (Wang's choice) as a function of the redshift for different values of (w_0, w_a). In the lower panel, we show the same ratio for the case $\langle\psi(z)\rangle = \psi(z_v)$. For notational clarity, we indicate those ratios by

$$\frac{r_v}{r_{\rm ta}} \equiv \begin{cases} x & \text{if } \eta = 1, \\ y & \text{if } \eta = \frac{(1+3w_v)\rho_{\rm DE}(z_v)}{(1+3w_{\rm ta})\rho_{\rm DE}(z_{\rm ta})}, \end{cases} \tag{C.21}$$

where $w_v = w(z_v)$. For $z \gg 1$, where dark energy effects can be neglected, the ratio of the virial to the turn-around radii approaches, as expected, the asymptotic Einstein–de Sitter value $x = 1/2$. The variations of x with the choice of the functional form of the deviation parameter η are of order of a few percent. The resulting analysis on the growth of massive galaxy clusters does not appreciably depend on η, and the results presented in the previous sections are for the case $\eta = 1$.

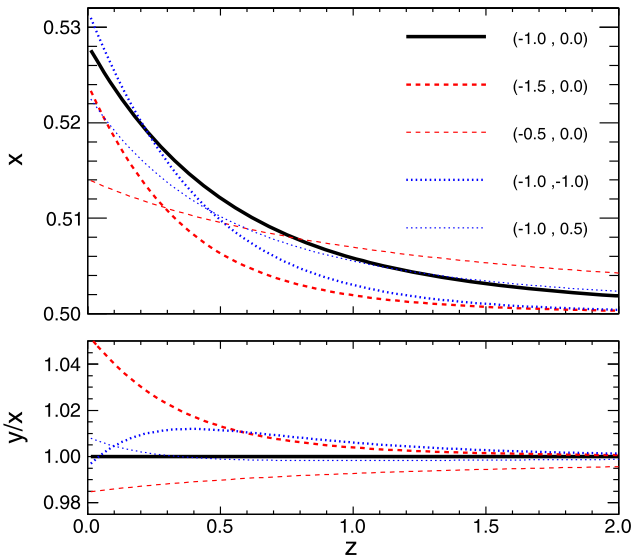

Fig. 9 *Upper panel*. The ratio of the virial radius to the turn-around radius, $x \equiv r_v/r_{\rm ta}$ with $\eta = 1$ (corresponding to Wang's choice), as a function of the redshift for different values of (w_0, w_a) (the same as in Fig. 1). *Lower panel*. The ratio of x to y, where $y \equiv r_v/r_{\rm ta}$ with η defined in Eq. (C.21). In both panels, we fixed $\Omega_m = 0.27$

References

1. S.W. Allen, A.E. Evrard, A.B. Mantz, arXiv:1103.4829 [astro-ph.CO]
2. P.J.E. Peebles, Astrophys. J. **284**, 439 (1984)
3. S. Weinberg, *Cosmology* (Oxford University Press, New York, 2008)
4. G.M. Voit, Rev. Mod. Phys. **77**, 207 (2005). arXiv:astro-ph/0410173
5. P. Brax, arXiv:0912.3610 [astro-ph.CO]
6. J.-P. Uzan, arXiv:0912.5452 [gr-qc]
7. A. De Felice, S. Tsujikawa, Living Rev. Relativ. **13**, 3 (2010). arXiv:1002.4928 [gr-qc]
8. E.V. Linder, arXiv:1004.4646 [astro-ph.CO]
9. A. Blanchard, Astron. Astrophys. Rev. **18**, 595 (2010). arXiv:1005.3765 [astro-ph.CO]
10. D. Sapone, Int. J. Mod. Phys. A **25**, 5253 (2010). arXiv:1006.5694 [astro-ph.CO]
11. H.K. Jassal, J.S. Bagla, T. Padmanabhan, Mon. Not. R. Astron. Soc. **405**, 2639 (2010). arXiv:astro-ph/0601389
12. K.M. Wilson, G. Chen, B. Ratra, Mod. Phys. Lett. A **21**, 2197 (2006). arXiv:astro-ph/0602321
13. T.M. Davis et al., Astrophys. J. **666**, 716 (2007). arXiv:astro-ph/0701510
14. P.J.E. Peebles, B. Ratra, Rev. Mod. Phys. **75**, 559 (2003). arXiv:astro-ph/0207347
15. L. Perivolaropoulos, J. Phys. Conf. Ser. **222**, 012024 (2010). arXiv:1002.3030 [astro-ph.CO]
16. P.J.E. Peebles, B. Ratra, Astrophys. J. Lett. **325**, L17 (1988)
17. B. Ratra, P.J.E. Peebles, Phys. Rev. D **37**, 3406 (1988)
18. A. Mantz, S.W. Allen, H. Ebeling, D. Rapetti, Mon. Not. R. Astron. Soc. **387**, 1179 (2008). arXiv:0709.4294 [astro-ph]
19. A. Mantz, S.W. Allen, D. Rapetti, H. Ebeling, Mon. Not. R. Astron. Soc. **406**, 1759 (2010). arXiv:0909.3098 [astro-ph.CO]
20. A. Vikhlinin et al., Astrophys. J. **692**, 1060 (2009). arXiv:0812.2720 [astro-ph]
21. N.A. Arhipova, T. Kahniashvili, V.N. Lukash, Astron. Astrophys. **386**, 775 (2002). arXiv:astro-ph/0110426
22. T. Kahniashvili, E. von Toerne, N.A. Arhipova, B. Ratra, Phys. Rev. D **71**, 125009 (2005). arXiv:astro-ph/0503328
23. E. Rozo et al., Astrophys. J. **708**, 645 (2010). arXiv:0902.3702 [astro-ph.CO]
24. S. Basilakos, M. Plionis, J.A.S. Lima, Phys. Rev. D **82**, 083517 (2010). arXiv:1006.3418 [astro-ph.CO]
25. M. Manera, D.F. Mota, Mon. Not. R. Astron. Soc. **371**, 1373 (2006). astro-ph/0504519

26. S. Basilakos, M. Plionis, J. Sola, Phys. Rev. D **80**, 083511 (2009). arXiv:0907.4555 [astro-ph.CO]
27. J. Grande, J. Sola, S. Basilakos, M. Plionis, J. Cosmol. Astropart. Phys. **1108**, 007 (2011). arXiv:1103.4632 [astro-ph.CO]
28. N.A. Bahcall, X.-h. Fan, Astrophys. J. **504**, 1 (1998). arXiv:astro-ph/9803277
29. N.A. Bahcall, P. Bode, Astrophys. J. **588**, L1 (2003). arXiv:astro-ph/0212363
30. M. Chevallier, D. Polarski, Int. J. Mod. Phys. D **10**, 213 (2001). arXiv:gr-qc/0009008
31. E.V. Linder, Phys. Rev. Lett. **90**, 091301 (2003). arXiv:astro-ph/0208512
32. L.R. Abramo, R.C. Batista, R. Rosenfeld, J. Cosmol. Astropart. Phys. **0907**, 040 (2009). arXiv:0902.3226 [astro-ph.CO]
33. S. Podariu, T. Souradeep, J.R. Gott, B. Ratra, M.S. Vogeley, Astrophys. J. **559**, 9 (2001). arXiv:astro-ph/0102264
34. E. Komatsu et al. (WMAP Collaboration), Astrophys. J. Suppl. Ser. **192**, 18 (2011). arXiv:1001.4538 [astro-ph.CO]
35. W.H. Press, P. Schechter, Astrophys. J. **187**, 425 (1974)
36. R.K. Sheth, G. Tormen, Mon. Not. R. Astron. Soc. **308**, 119 (1999). arXiv:astro-ph/9901122
37. D.J. Eisenstein, W. Hu, Astrophys. J. **496**, 605 (1998). arXiv:astro-ph/9709112
38. Y. Ikebe, T.H. Reiprich, H. Boehringer, Y. Tanaka, T. Kitayama, Astron. Astrophys. **383**, 773 (2002). arXiv:astro-ph/0112315
39. J.P. Henry, Astrophys. J. **534**, 565 (2000). arXiv:astro-ph/0002365
40. M. Schmidt, Astrophys. J. **151**, 393 (1968)
41. Y. Avni, J.N. Bahcall, Astrophys. J. **235**, 694 (1980)
42. M. Donahue, G.M. Voit, I.M. Gioia, G. Luppino, J.P. Hughes, J.T. Stocke, arXiv:astro-ph/9707010
43. J. Hjorth, J. Oukbir, E. van Kampen, New Astron. Rev. **42**, 145 (1998)
44. J. Hjorth, J. Oukbir, E. van Kampen, Mon. Not. R. Astron. Soc. **298**, L1 (1998). arXiv:astro-ph/9802293
45. P.E.J. Nulsen, S.L. Powell, A. Vikhlinin, Astrophys. J. **722**, 55 (2010). arXiv:1008.2393 [astro-ph.CO]
46. G.L. Fogli, E. Lisi, A. Marrone, D. Montanino, A. Palazzo, Phys. Rev. D **66**, 053010 (2002). arXiv:hep-ph/0206162
47. E. Gaztañaga, A. Cabré, L. Hui, Mon. Not. R. Astron. Soc. **399**, 1663 (2009). arXiv:0807.3551 [astro-ph]
48. L. Samushia, B. Ratra, Astrophys. J. **701**, 1373 (2009). arXiv:0810.2104 [astro-ph]
49. Y. Wang, Mod. Phys. Lett. A **25**, 3093 (2010), and references therein, arXiv:0904.2218 [astro-ph.CO]
50. W.J. Percival et al. (SDSS Collaboration), Mon. Not. R. Astron. Soc. **401**, 2148 (2010). arXiv:0907.1660 [astro-ph.CO]
51. E.W. Kolb, M.S. Turner, *The Early Universe* (Addison-Wesley, Redwood City, 1990)
52. P.S. Corasaniti, A. Melchiorri, Phys. Rev. D **77**, 103507 (2008). arXiv:0711.4119 [astro-ph]
53. G. Chen, B. Ratra, Publ. Astron. Soc. Pac. **123**, 1127 (2011). arXiv:1105.5206 [astro-ph.CO]
54. G. Chen, J.R. Gott, B. Ratra, Publ. Astron. Soc. Pac. **115**, 1269 (2003). arXiv:astro-ph/0308099
55. G.A. Tamman, A. Sandage, B. Reindl, Astron. Astrophys. Rev. **15**, 289 (2008). arXiv:0806.3018 [astro-ph]
56. W.L. Freedman, B.F. Madore, Annu. Rev. Astron. Astrophys. **48**, 673 (2010). arXiv:1004.1856 [astro-ph.CO]
57. R. Jimenez, A. Loeb, Astrophys. J. **573**, 37 (2002). arXiv:astro-ph/0106145
58. D. Stern, R. Jimenez, L. Verde, M. Kamionkowski, S.A. Stanford, J. Cosmol. Astropart. Phys. **1002**, 008 (2010). arXiv:0907.3149 [astro-ph.CO]
59. E. Gaztañaga, A. Cabré, L. Hui, Mon. Not. R. Astron. Soc. **399**, 1663 (2009). arXiv:0807.3551 [astro-ph]
60. L. Samushia, B. Ratra, Astrophys. J. Lett. **650**, L5 (2006). arXiv:astro-ph/0607301
61. H. Zhang, Z.-H. Zhu, J. Cosmol. Astropart. Phys. **0803**, 007 (2008). arXiv:astro-ph/0703245
62. A.A. Sen, R.J. Scherrer, Phys. Lett. B **659**, 457 (2008). arXiv:astro-ph/0703416
63. L. Samushia, G. Chen, B. Ratra, arXiv:0706.1963 [astro-ph]
64. N. Pan, Y. Gong, Y. Chen, Z.-H. Zhu, Class. Quantum Gravity **27**, 155015 (2010). arXiv:1005.4249 [astro-ph.CO]
65. Y. Chen, B. Ratra, Phys. Lett. B **703**, 406 (2011), and references therein. arXiv:1106.4294 [astro-ph.CO]
66. R. Amanullah et al., Astrophys. J. **716**, 712 (2010). arXiv:1004.1711 [astro-ph.CO]
67. J. Guy et al., Astron. Astrophys. **466**, 11 (2007). arXiv:astro-ph/0701828
68. A. Lewis, S. Bridle, Phys. Rev. D **66**, 103511 (2002). arXiv:astro-ph/0205436
69. L. Campanelli, P. Cea, G.L. Fogli, A. Marrone, Phys. Rev. D **83**, 103503 (2011). arXiv:1012.5596 [astro-ph.CO]
70. K.-H. Chae, G. Chen, B. Ratra, D.-W. Lee, Astrophys. J. Lett. **607**, L71 (2004). arXiv:astro-ph/0403256
71. S. Lee, K.-W. Ng, Phys. Rev. D **76**, 043518 (2007). arXiv:0707.1730 [astro-ph]
72. M. Yashar, B. Bozek, A. Abrahamse, A. Albrecht, M. Barnard, Phys. Rev. D **79**, 103004 (2009). arXiv:0811.2253 [astro-ph]
73. M. Biesiada, A. Piorkowska, B. Malec, Mon. Not. R. Astron. Soc. **406**, 1055 (2010), and references therein. arXiv:1105.0946 [astro-ph.CO]
74. S. Eidelman et al. (Particle Data Group), Phys. Lett. B **592**, 1 (2004)
75. P. Schuecker, H. Bohringer, C.A. Collins, L. Guzzo, Astron. Astrophys. **398**, 867 (2003). arXiv:astro-ph/0208251
76. A.G. Riess et al., Astrophys. J. **730**, 119 (2011) [Erratum-ibid. **732**, 129 (2011)]. arXiv:1103.2976 [astro-ph.CO]
77. L.I. Gurvits, K.I. Kellermann, S. Frey, Astron. Astrophys. **342**, 378 (1999). arXiv:astro-ph/9812018
78. E.J. Guerra, R.A. Daly, L. Wan, Astrophys. J. **544**, 659 (2000). arXiv:astro-ph/0006454
79. G. Chen, B. Ratra, Astrophys. J. **582**, 586 (2003). arXiv:astro-ph/0207051
80. M. Bonamente, M.K. Joy, S.J. La Roque, J.E. Carlstrom, E.D. Reese, K.S. Dawson, Astrophys. J. **647**, 25 (2006). arXiv:astro-ph/0512349
81. Y. Chen, B. Ratra, arXiv:1105.5660 [astro-ph.CO], and references therein
82. S. Capozziello, V.F. Cardone, M. Funaro, S. Andreon, Phys. Rev. D **70**, 123501 (2004). arXiv:astro-ph/0410268
83. N. Pires, Z.-H. Zhu, J.S. Alcaniz, Phys. Rev. D **73**, 123530 (2006). arXiv:astro-ph/0606689
84. L. Samushia, A. Dev, D. Jain, B. Ratra, Phys. Lett. B **693**, 509 (2010). arXiv:0906.2734 [astro-ph.CO]
85. M.A. Dantas, J.S. Alcaniz, D. Mania, B. Ratra, Phys. Lett. B **699**, 239 (2011), and references therein. arXiv:1010.0995 [astro-ph.CO]
86. S.W. Allen, D.A. Rapetti, R.W. Schmidt, H. Ebeling, G. Morris, A.C. Fabian, Mon. Not. R. Astron. Soc. **383**, 879 (2008). arXiv:0706.0033 [astro-ph]
87. L. Samushia, B. Ratra, Astrophys. J. Lett. **680**, L1 (2008). arXiv:0803.3775 [astro-ph]
88. S. Ettori et al., Astron. Astrophys. **501**, 61 (2009), and references therein. arXiv:0904.2740 [astro-ph.CO]
89. B.E. Schaefer, Astrophys. J. **660**, 16 (2007). arXiv:astro-ph/0612285
90. N. Liang, S.N. Zhang, AIP Conf. Proc. **1065**, 367 (2008). arXiv:0808.2655 [astro-ph]
91. Y. Wang, Phys. Rev. D **78**, 123532 (2008). arXiv:0809.0657 [astro-ph]

92. L. Samushia, B. Ratra, Astrophys. J. **714**, 1347 (2010), and references therein. arXiv:0905.3836 [astro-ph.CO]
93. V. Barger, E. Guarnaccia, D. Marfatia, Phys. Lett. B **635**, 61 (2006). arXiv:hep-ph/0512320
94. R.R. Caldwell, E.V. Linder, Phys. Rev. Lett. **95**, 141301 (2005). arXiv:astro-ph/0505494
95. G. Gupta, S. Majumdar, A.A. Sen, Mon. Not. R. Astron. Soc. **420**, 1309 (2012). arXiv:1109.4112 [astro-ph.CO]
96. R.J. Scherrer, Phys. Rev. D **73**, 043502 (2006). arXiv:astro-ph/0509890
97. C. Armendariz-Picon, V.F. Mukhanov, P.J. Steinhardt, Phys. Rev. Lett. **85**, 4438 (2000). arXiv:astro-ph/0004134
98. T. Chiba, Phys. Rev. D **73**, 063501 (2006) [Erratum-ibid. D **80**, 129901 (2009)]. arXiv:astro-ph/0510598
99. A.Y. Kamenshchik, U. Moschella, V. Pasquier, Phys. Lett. B **511**, 265 (2001). arXiv:gr-qc/0103004
100. M.C. Bento, O. Bertolami, A.A. Sen, Phys. Rev. D **66**, 043507 (2002). arXiv:gr-qc/0202064
101. B. Ratra, Phys. Rev. D **43**, 3802 (1991)
102. S. Podariu, B. Ratra, Astrophys. J. **532**, 109 (2000). arXiv:astro-ph/9910527
103. F. Pace, J.C. Waizmann, M. Bartelmann, arXiv:1005.0233 [astro-ph.CO]
104. D.F. Mota, J. Cosmol. Astropart. Phys. **0809**, 006 (2008). arXiv:0812.4493 [astro-ph]
105. J.F. Navarro, C.S. Frenk, S.D.M. White, Mon. Not. R. Astron. Soc. **275**, 720 (1995). arXiv:astro-ph/9408069
106. J.S. Bullock et al., Mon. Not. R. Astron. Soc. **321**, 559 (2001). arXiv:astro-ph/9908159
107. P. Wang, Astrophys. J. **640**, 18 (2006). arXiv:astro-ph/0507195